Politecnico di Torino

Implementation of a multibody model as digital twin for a robotic arm

Supervisors:

Prof.ssa Mara Terzini

Ing. Giovanni Putame

Ing. Simone Borrelli

Ing. Marco Daghero

Candidate:

Fulvia Tedesco

July 2024

Abstract

Purpose: The aim of this thesis is to implement, develop and validate the digital twin of the collaborative robot Doosan H2515, used for handling tools and accessories during various industrial procedures. The objective is to enable precise execution of motion laws by the robotic arm and to manage the physical system from its digital counterpart, in order to facilitate its application in the medical-surgical domain, requiring utmost accuracy and movement exactitude.

Methods: A multibody model of the cobot is constructed, comprising six distinct components.

The parts are modeled as rigid bodies, and physical and mechanical properties are assigned to each. Key properties include mass, center of mass and inertia. To achieve a system of point masses, inertia is set to zero for all parts of the system.

Junctions between components are modeled by creating joints, placed at the interface between adjacent parts. Specifically, the model consists of a system with six joints, all of which are single-degree-of-freedom revolute joints. This means that they allow only revolution around the axis of rotation of the corresponding part, preventing all other movements. Angular and torque measurements are then created for each joint, enabling monitoring of the relevant quantities of the model under examination.

The defined digital twin is validated through parallel experimental tests and numerical simulations, employing the *Adams View* software environment, and comparing the results derived from both approaches. More specifically, to test the behavior of the cobot, static, kinematic, and dynamic simulations were performed, with an increasing degrees of complexity. Statics and kinematics tests were initially studied by moving the joints separately; dynamics tests permitted to better investigate on the internal torques generated at each joints. In that sense, an experimental test was designed to verify the digital twin confidence in replicating a motion controlled dynamics.

Results: The results from these analyses indicate that the static and kinematic behavior of the Doosan H2515 is accurately estimated by the digital twin. However, issues arise in dynamic simulations, particularly in terms of constraint reactions. A deviation is observed between *Joint Torque* experimental and numerical results. The analytical correspondence

with the *in silico* model, arises the hypothesis that the deviation could be attributed to the presence of internal brakes (elements not replicated in the digital model) whose loads and control algorithm cannot be extracted and then difficult to be estimated. Observing the joints involved in the bending of the robotic arm (Joint 2, 3, 5) this deviation appears more pronounced closer to the base due to the increased weight of downstream components; thus, Joint 2 is identified as the 'critical joint'.

Finally, Joints 1 and 6 were not validated, due to the difficulty in controlling experimental loads along their axis. The primary focus was then maintained on the joints involved in the bending of the robotic arm.

Table of Contents

List of Figures

List of Tables

Introduction

The Doosan H2515 robotic arm is a type of collaborative robot designed and manufactured by Doosan Robotics. It is engineered to operate in environments where humans and robots collaborate, ensuring safe and efficient interactions between operators and the machine.

The collaborative robotic arm Doosan H2515 is primarily designed for industrial applications, where its ability to work safely alongside humans is particularly useful. However, collaborative robots in general are finding increasingly diverse applications, including in the healthcare, hospital, and medical fields. Despite its potential, there is no specific public information indicating an extensive use of the Doosan H2515 in hospitals, but the versatility of cobots suggests that, with the right modifications and approvals, it could be possible.

This collaborative arm comprises multiple joints facilitating the robot's movement and manipulation of objects in diverse manners. Its structure encompasses a stationary base unit, from which the movable components extend. Each component consists of several segments interconnected by joints enabling motion.

Overall, creating a digital twin of a robotic arm presents an advanced approach to designing, analyzing, monitoring, and optimizing robotic systems, maximizing their value and performance. Moreover, achieving a sufficiently high level of accuracy can thereby warrant the adoption of such a system within hospital environment and thus, for biomedical applications as well.

Generally, multibody models find extensive use in robotics and various other engineering disciplines for designing, optimizing, and analyzing the behavior of complex systems before their physical implementation. Therefore, the initial step towards creating a digital twin of the Doosan H2515 robotic arm involves developing its multibody model.

For the implementation and validation of the multibody model, simulations are conducted simultaneously in both experimental and numerical environments, and the results obtained

are compared. Experimental simulations entail direct execution on the actual physical system, while *Adams View* software has been chosen as the numerical environment for the development and validation of the digital twin.

The thesis is structured as follows:

Chapter 1 serves as the foundational stage for the development of this thesis. It begins with a broad overview of the macro-category of devices encompassing the Doosan H2515: collaborative robots. Subsequently, the discussion delves into the specific model under examination, elucidating its key functional and structural attributes.

Chapter 2 outlines the workflow required to develop the multibody model of the robotic arm. It focuses on the physical construction of the constituent parts, their connections and the definition of key mechanical quantities, with particular emphasis on the torques measured on the joints.

In *Chapter 3*, the static validation of the cobot is conducted. For this purpose, reference configurations are defined and simulated in both experimental and numerical environments, with the respective torques measured. The obtained results are then compared with those derived from the analytical solution of the system's statics.

In *Chapter 4*, the kinematics of the robotic arm are studied by assigning a motion to the system and analyzing the trajectory followed over time by its *End Effector*.

Chapter 5 and *Chapter 6* analyze the assignment and execution of a specific movement by the cobot. The distinction between the two analyses lies in the method of motion assignment: in Chapter 4, a displacement law is employed as the motion model; whereas in the subsequent chapter, motion is defined by a velocity law. Regardless, in both scenarios, the motion law is delineated employing a ramp function.

Chapter 7 evaluates the simulation of a constant force application. The analysis primarily revolves around examining the torques measured on the cobot's joints under static conditions when subjected to a constant external force.

In *Chapter 8*, a comprehensive investigation is conducted to grasp the functioning of Joint 2, leveraging the ambiguities revealed in the results from prior simulations as a starting point. The primary focus lies in unraveling the influence of the respective motor and brake actions on the experimentally measured torque, and subsequently, understanding the observed deviation from the numerically detected torque.

Chapter 1

Doosan H2515 robotic arm

In the initial sections of this chapter, an examination of collaborative robotic arms is undertaken.

Following this broad overview, the focus gradually narrows to a specific series, with particular emphasis on the Doosan H2515 model, which is highlighted as the primary subject of this thesis.

Moving forward, an in-depth exploration ensues, delving into the intricate and complex details of the system's structure and architecture – in order to achieve a profound understanding of the operational dynamics of the system. This foundational understanding is essential to facilitate a detailed and informed discussion in the later sections of the chapter.

1.1 Introduction to collaborative robot

1.1.1 What is a collaborative robot

Collaborative robots, introduced to the market by Universal Robots in 2008, are anthropomorphic robots[1] equipped with movements across six axes. They are specifically designed to adhere to safety, flexibility, and compactness criteria, allowing them to work in close proximity to operators even without protective barriers indoors [11] [27].

---

[1]: Anthropomorphic robots, characterized by movements across 5 or more axes, bear resemblance to the human arm both in form and articulation capabilities. Hence, they are commonly referred to as anthropomorphic robotic arms.

The distinctions between traditional robots and collaborative robots can be summarized, in simplified terms, by the following properties:

- Safety;
- Flexibility;
- Deployment speed.

Most collaborative robots can operate without the need for protective barriers, unlike traditional robots which require costly fencing to separate the workspace from human interaction. This is not only due to size and speed (which are generally more limited compared to traditional robots) but primarily because of a different conception of the robot's function [2] [5].

Collaborative robots come equipped with a series of inherent *natives safety*[2] that allow for installation and programming to view the process directly as an activity shared between humans and cobots. With a cobot, it is possible to set parameters such as distance and stopping time, among many other variables, ensuring its implementation remains entirely safe even in crowded environments. Furthermore, collaborative robots offer the possibility of being equipped with a wide range of sensors that enhance safety, such as vision systems that detect the presence of operators by monitoring movements and reaction times of the cobot [3].

The automation facilitated by a traditional robot tends to be inflexible. Conversely, flexibility is the defining feature of a collaborative robot. A cobot's compact and lightweight design allows for easy relocation within the industrial layout, precisely where it is needed. Moreover, its versatility enables it to perform a variety of tasks, serving as a versatile arm adaptable to diverse operational needs [8] [9].

The ease of programming is another characteristic that underscores the flexibility of cobots.

What truly makes cobots a plug-and-play solution capable of enhancing production lines and processes is their deployment speed, which is the culmination of several factors. On one hand, cobots require minimal, cost-effective modifications to production layouts and can be swiftly integrated into work areas, owing to their compact size and inherent safety

---

[2] '*Native safety*' refers to inherent safety features designed directly into the system of a collaborative robot. These include integrated sensors, advanced control systems, and technologies enabling the robot to detect human presence nearby and react appropriately to avoid collisions or damage.

features. On the other hand, powered by standard 220V electrical current, they are virtually integrable anywhere, including civilian environments [19] [20].

1.1.2 Applications of collaborative robots

Cobots excel in automating a diverse array of applications. Their simplicity and quick programming make them versatile tools ready to swiftly transition between tasks and enter production seamlessly.

Besides being employed in strictly industrial applications such as Pick and Place, assembly, and quality control, collaborative robots are finding increasing use in various sectors due to their safety, flexibility, and ease of use. They are rapidly spreading in the medical, surgical, and rehabilitative fields, where they offer innovative solutions that enhance operational efficiency and the quality of care [12] [16]:

- Medical Field: Patient assistance and laboratory analysis and testing.
  Patient assistance: Cobots can assist patients with reduced mobility by helping with daily tasks such as medication administration or movement support. This can reduce the workload of healthcare staff and improve the quality of life for patients [13];
  Laboratory analysis and testing: In laboratory settings, cobots are used to automate repetitive processes such as sample handling and testing. For example, the University Hospital of Copenhagen has integrated cobots to manage blood samples, improving efficiency and reducing response times [21];
- Surgical field/robotic surgery: Cobots can support less invasive surgical operations, assisting medical staff in delicate activities. While specialized surgical robots (such as the Da Vinci Surgical System) dominate this field, cobots offer potential for assisted surgical interventions, ensuring precision and reducing operator fatigue [1] [18];
- Rehabilitation field/rehabilitation therapies: Cobots are used in rehabilitation therapies to provide assisted physical exercises for patients recovering from injuries. They can be programmed to adapt to the specific needs of the patient, personalizing treatments [14] [15].

In conclusion, an application managed jointly by an operator and a collaborative robot is 85% more productive than a fully automated or entirely manual application. This is due to the cobot's ability to effectively blend human effort with the precision of automation [10].

1.2 Doosan H2515: Architecture and Design

This thesis examines the Doosan H2515 collaborative robotic arm, which belongs to the H series recently introduced by Doosan Robotics.

The introduction of the H-SERIES has sparked interest due to its highest payload capacity on the market – up to 25 kg [26]. This represents a significant increase compared to existing cobots, which typically support payloads of around 15 kg. Moreover, the H-SERIES cobots boast a 1700 mm reach, enhancing positioning effectiveness by combining their high payload capacity with precision provided by six integrated load cells in their joints.

In addition to payload capacity, the H-SERIES has bolstered safety controls with the best collision sensitivity in its category, powered by six torque sensors and a gravity compensation algorithm.

Adding to its high-end features, the H-SERIES offers greater flexibility with only half the weight of other cobots in the same class.

Moreover, H-SERIES cobots can handle multiple objects simultaneously due to its high payload capacity, boosting productivity by reducing object movement time. Furthermore, it enables the installation of multiple tools at once, eliminating the need for frequent replacements and thereby enhancing overall productivity [22].

The foundational components of the Doosan H2515 robotic arm include [22]:

1. Robotic Arm: the Doosan H2515 is equipped with a robotic arm that extends from a fixed base (Figure 1). Comprised of a series of joints, it facilitates multi-axial movements, enabling the robot to attain various positions within the workspace with precision and flexibility:

Figure 1 Doosan H2515 Collaborative Robot

2. Joints: engineered to deliver flexibility in motion, the robot's joints are individually controlled by electric motors or hydraulic drives. This design ensures the execution of accurate and seamless movements;

3. Actuators: positioned at each joint, the actuators of the robot are responsible for transmitting motion to different parts of the arm, facilitating smooth and efficient operation;

4. Brakes: brakes are installed on specific parts of the robot. For the model being discussed, brakes are positioned at each joint of the system to ensure safety during operation. For instance, emergency brakes can be activated in case of power loss or other malfunctions to keep the robot in a stable and secure position;

5. Terminal *End Effector*: located at the end of the robotic arm, the Terminal *End Effector* (Figure 2) is the component that directly interacts with the surrounding environment. Various tools can be attached to this part of the system to perform specific tasks. For example, a force sensor (like a load cell) can be affixed to the *End Effector* to measure the forces exerted by the cobot component when in contact with objects. Alternatively, a gripper can be mounted for object manipulation, a suction cup for lifting flat objects, or other specialized tools for specific tasks:

Figure 2 Doosan H2515 End Effector

6. Direct Teaching Button: this button facilitates the selection of various teaching modes and the saving of coordinates through simple button operations:

Figure 3 Doosan H2515 Direct Teaching Button

7. Control System/Controller: the Doosan H2515 is equipped with an advanced control system responsible for managing the robot's movements and interactions with its surrounding environment. This system can be programmed to execute a wide range of tasks using specific programming languages or intuitive user interfaces. Additionally, it seamlessly interfaces with various automation equipment and peripherals, supporting a comprehensive suite of the latest communication technologies:

Figure 4 Doosan H2515 Control System

8. Safety Sensors: the Doosan H2515 robot comes equipped with a set of safety sensors designed to continuously monitor its surrounding environment for the presence of obstacles or individuals nearby. These sensors are programmed to promptly halt the robot's movements upon detecting potential hazards, thereby playing a crucial role in ensuring the safety of human operators working in close proximity to the robot;

9. Teach Pendant: this device serves as an instructional tool with an intuitive user interface, offering user-friendly operation akin to that of a tablet PC. Enhanced with the DART platform, it simplifies programming, monitors robot activities, and configures various applications seamlessly. This interface streamlines human-machine interaction and facilitates the robot's integration into industrial operations:

Figure 5 Doosan H2515 Teach Pendant

10. Emergency Stop Button: this is located on the interface of the Teach Pendant.
If this button is not unlocked, the robot's movement is prevented, even if an attempt is made to operate it from the *DART Studio* platform. Furthermore, the safety button can halt the robot in an emergency situation to prevent accidents.

9

Chapter 2

Methods

This chapter will begin upon the process of formulating and refining the multibody model designed specifically for the Doosan H2515 robotic arm.

In the pursuit of establishing a fully realized digital twin for this collaborative robot, it becomes imperative to meticulously attribute a comprehensive spectrum of physical and mechanical attributes to each of its constituent components. Moreover, the precise quantification of torque measurements is indispensable in this endeavor.

These quantitative parameters assume a paramount significance as they are instrumental not only in ensuring the cobot's adeptness in maintaining designated positions but also in facilitating its execution of predetermined movements with utmost accuracy and efficiency.

2.1 Development of the digital twin

The development of the digital twin proceeds through the following phases:

1. Construction of the cobot's multibody model in a numerical environment;
2. Simulation and analysis of movements performed by the cobot: in the numerical environment, utilizing the developed multibody model, and in the experimental environment, using the physical robot.
3. Comparison and critical evaluation of the results.

Within the software environment of *Adams View*, the construction of the multibody model for the Doosan H2515 robotic arm and the subsequent numerical simulation take place.

Adams View is a component of the Adams software suite, developed by *MSC Software.*

The *Adams* software is widely regarded as the gold standard in multi-body dynamic simulation. It specifically aids engineers in analyzing the dynamics of moving parts and the distribution of loads and forces within mechanical systems [24] [23].

In addition to numerical simulations, experimental simulations will be conducted using the actual Doosan H2515.
The experimental working environment is embodied by the *DART Studio* platform.
This software, provided by Doosan Robotics for designing and programming their robots, offers users advanced functionalities under the *DART* (Doosan Adaptive Robot Technology) *Studio* suite.
This platform empowers engineers to design and test work scenarios in a virtual setting before deploying them in real-world environments and allows extracting three fundamental measures of the main quantity of interest, which as mentioned is the torque measured on the joints:

- 'External Joint Torque': torque (measured on the joints) solely due to the presence of external forces applied to the cobot. In other words, it is the torque exerted by each joint to counteract the action of external loads;
- 'Joint Torque Sensor': torque (measured on the joints) that takes into account both the presence of external forces applied to the cobot and the weight of various parts of the system. In this case, the torque measured on each joint reflects not only balancing external forces but also supporting the weight of each component;
- 'Joint Model Torque': torque (measured on the joints) exclusively related to the weight of the cobot's components.

Where the third quantity can be derived as the algebraic sum of the first two.

Among the three experimental quantities available, the one compared with the numerical measurement is 'Joint Model Torque'. This choice is made because in the experimental environment, a load cell is applied at the *End Effector* of the cobot (necessary for measuring external forces), which is not replicated in the numerical model. In other words, in the numerical environment, the torque measurement accounts solely for the weight of the cobot's parts.
For this reason, attention is focused on measuring the torques exerted by the joints of the system, solely to support the weight of each component – 'Joint Model Torque'.

Both in the experimental and numerical scenarios, specific movements performed by the cobot need to be simulated.

In the experimental environment, movement assignment is carried out using the DART Studio platform, which allows setting: the angular values of the joints that define the initial and final positions, as well as the values of speed and acceleration.

Conversely, in the numerical environment, movement is assigned by defining a motion law, which can be a displacement, velocity, or acceleration law. In any case, a step function has been chosen to achieve smoother movement. Equation 2.1 provides an example of the motion law expressed in terms of displacement:

$$displacement(time) = step(x, x_0, h_0, x_1, h_1) \qquad \text{(Equation 2.1)}$$

Where:

- x: independent variable, *time*;
- h: dependent variable, *angular displacement*;
- x_0 = starting instant of motion;
- x_1 = final instant of motion;
- h_0 = initial condition of angular displacement;
- h_1 = final condition of angular displacement.

2.2 Pipeline (experimental e numerical)

Figure 6 illustrates the flowchart of the simulations to be conducted for advancing the implementation and validation of the digital twin of the Doosan H2515 collaborative robotic arm – both in experimental and numerical environment:

12

STATIC SIMULATIONS	KINEMATIC SIMULATIONS	DYNAMIC SIMULATIONS	FINAL SIMULATIONS
Study of the torques acting on the robotic arm under static equilibrium conditions.	Analysis of the trajectory followed by the End Effector during motion.	Analysis of the digital twin's capability to perform motion controlled dynamics.	Detailed investigation of the behavior of the 'critical joint' of the system, Joint 2.

Figure 6 Simulation Pipeline

Firstly, the statics of the cobot are studied. Specifically, the cobot is placed in specific configurations, and the torque exerted by the joints to maintain that position is measured accordingly.

Subsequently, movements are initiated within the system, leading to kinematic simulations and dynamic simulations. Kinematic simulations determine the *End Effector* position and orientation during the executed movement, whereas dynamic simulations focus on measuring the torques that the joints must exert to enable a specified motion.

Another aspect examined is the analysis of key quantities concurrently with the application of an external force.

The final step of the conducted work involves a detailed investigation of the operation of Joint 2, as all mentioned simulations highlight critical aspects in the behavior of this system component.

2.3 Multibody model construction

A multi-body model is a mathematical representation of a mechanical system composed of multiple rigid or deformable bodies interconnected through joints, hinges, constraints, and other components.

The multi-body model serves to simulate and analyze the dynamic behavior of complex systems in motion, enabling an understanding of how different components interact under external forces, gravity, and motion constraints. Additionally, it facilitates the assessment of how variations in system parameters, such as mass, geometry, stiffness, and friction, affect overall system performance.

Doosan H2515 cobot consists of six parts, as shown in Figure 7:
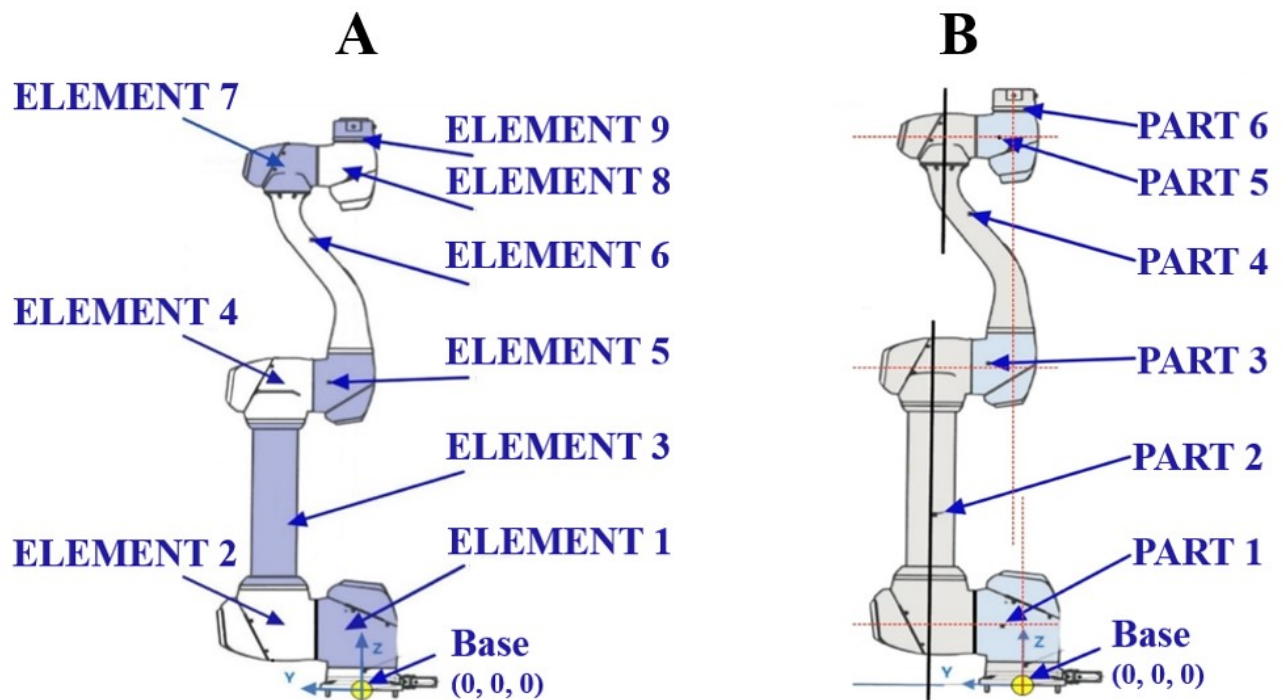
Figure 7 Doosan H2515 Structure

When importing the robot geometry into *Adams View* software, its structure is not automatically organized into the six parts shown in Figure 7 – B. In fact, the various components of the robot are initially separated into multiple segments, as shown in Figure 7 – A.

Therefore, it is necessary to manually connect the various elements of the robot until achieving a configuration where the constituent parts are six and arranged exactly as depicted in Figure 7 – B.

Table 1 Division of the elements of the Doosan H2515

PART #	COMPONENTS	Mass [kg]	*Center of Mass* [mm]
#1	Element 1	20.25	(-0.05, 118.54, 284.32)
#2	Element 2, 3, 4	28.11	(-0.02, 235.17, 701.59)
#3	Element 5	6.42	(-0.07, 59.43. 1111.21)
#4	Element 6, 7	7.3	(0.08, 140.58, 1543.83)
#5	Element 8	4.1	(-0.06, 58.69, 1723.89)
#6	Element 9	0.9	(-0.03, 9.91, 1794.9)

The location of the *Center of Mass* has been defined with respect to the global reference system of the model, which is positioned at the base of the cobot – as shown in Figure 7.

In accordance with Table 1, the 'Unite two solids' boolean function is utilized to respectively connect: Element 2, 3, 4, and Element 6,7.
By following this procedure, the correct structure of the cobot is replicated.

After achieving the correct structure of the robot in the numerical environment, the initial step in constructing its multibody model involves assigning masses and inertial properties to each of its six components: these properties are those listed in Table 1.
In terms of inertia, it has been intentionally configured to zero for each component, thereby transforming the system into one composed of point masses. This choice is motivated by the absence of data regarding the inertial properties of the Doosan H2515.

Following this, the creation of joints linking each part to its adjacent counterpart becomes imperative.
A joint in a robot serves as a mechanical connection point between two movable parts, facilitating relative motion through the operation of actuators such as electric, pneumatic, or hydraulic motors. These joints enable various degrees of freedom, including rotation, translation, or a combination thereof, and play a crucial role in defining the configuration and kinematics of the robot.
The joints identified for constructing the multibody model of the examined robot are as follows in Table 2:

Table 2 Doosan H2515 Joints

JOINT #	PARTS CONNECTED #	JOINT LOCATION [mm]
#1	#1, Base	(0, 0, 219)
#2	#1, #2	(0, 129, 344.3)
#3	#2, #3	(0, 137, 1103.8)
#4	#3, #4	(0, 10, 1190)
#5	#4, #5	(0, 122, 1723.3)
#6	#5, #6	(0, 10, 1783.8)

Each of these is a *Revolute Joint*, namely a spherical joint. The location of each joint has been defined with respect to the global reference system of the model, which is positioned at the base of the cobot – as shown in Figure 7.

Figure 8 shows Doosan H2515 joints:
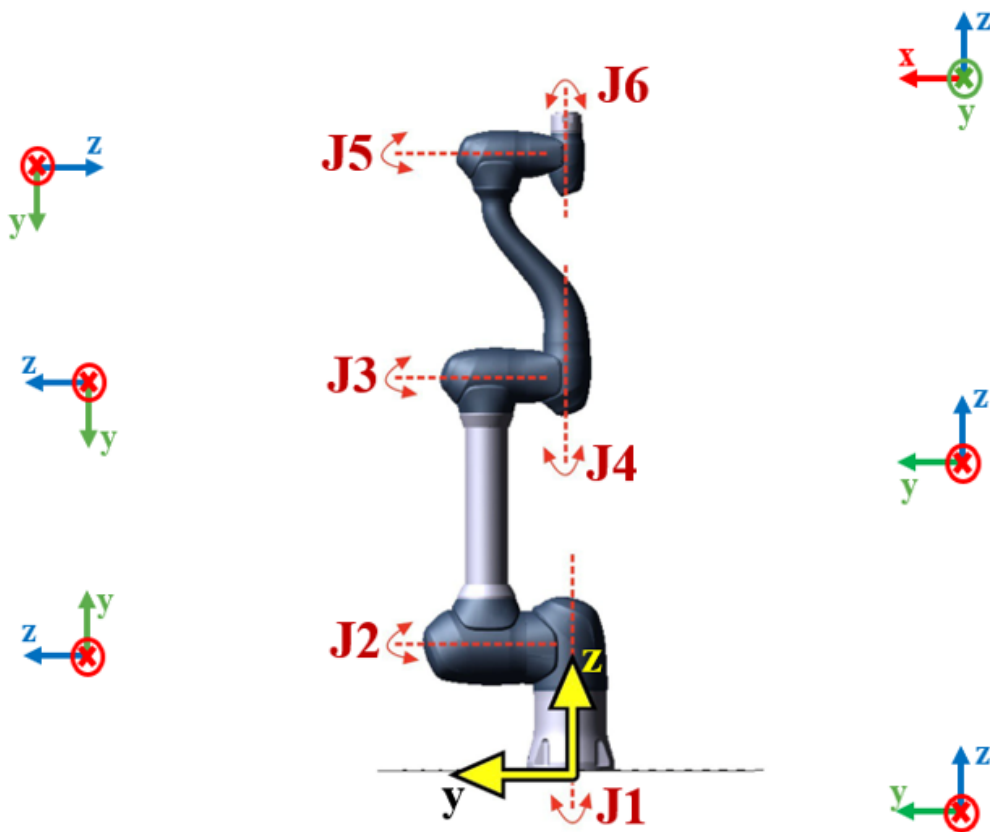
Figure 8 Doosan H2515 Joints

Spherical joints are characterized by a single degrees of freedom, enabling rotational motion around a specific axis.

Specifically, when considering the global reference system (shown in Figure 8): Joint 1, Joint 4 and Joint 6 allow rotation around the Z-axis; whereas Joint 2, Joint 3 and Joint 5 facilitate rotation around the Y-axis.

When creating joints, it is crucial to verify that their orientation is correct: each joint should be oriented to enable rotation around the positive axis of rotation of the corresponding part. To accomplish this, basic simulations are conducted in an experimental setting, during which the joints are individually moved by a few degrees. By determining the positive direction of rotation in the experimental setup, the joints of the numerical model are aligned accordingly, based on the observations made during the tests.

2.4 Creation of measurements

2.4.1 Creation of Joint Torque measurement

In order to conclude the construction of the model, it is necessary to create measurements of the quantities useful for describing the behavior of the cobot. In particular, the torques measured on the cobot's joints must be analyzed across various simulation scenarios.

Therefore, in the experimental environment, a movement is created from which the quantity of interest is then extracted.

Specifically, a movement of 30°/s is set and simulated for a time interval of 5s; the motion law is described in Equation 2.2:

$$displacement(time) = 30d*time \qquad \text{(Equation 2.2)}$$

To fully understand the characteristics of the movements under examination, it is essential to create measurements closely linked to them, specifically angular and torque measurements.

It is observed that: the created movement is associated with the joints, while the torque and angle measurements refer to the movement.

Since the motion of each joint predominantly occurs around the Z-axis of its local reference system (indicated in Figure 8), when creating the torque measurement associated with the joints, it is necessary to consider the 'Third Rotation Component'. This component effectively encapsulates the rotation occurring along the Z-axis of the local reference system of the respective joint.

Figure 9 illustrates the *Joint Torque* measured for both simulations described above:
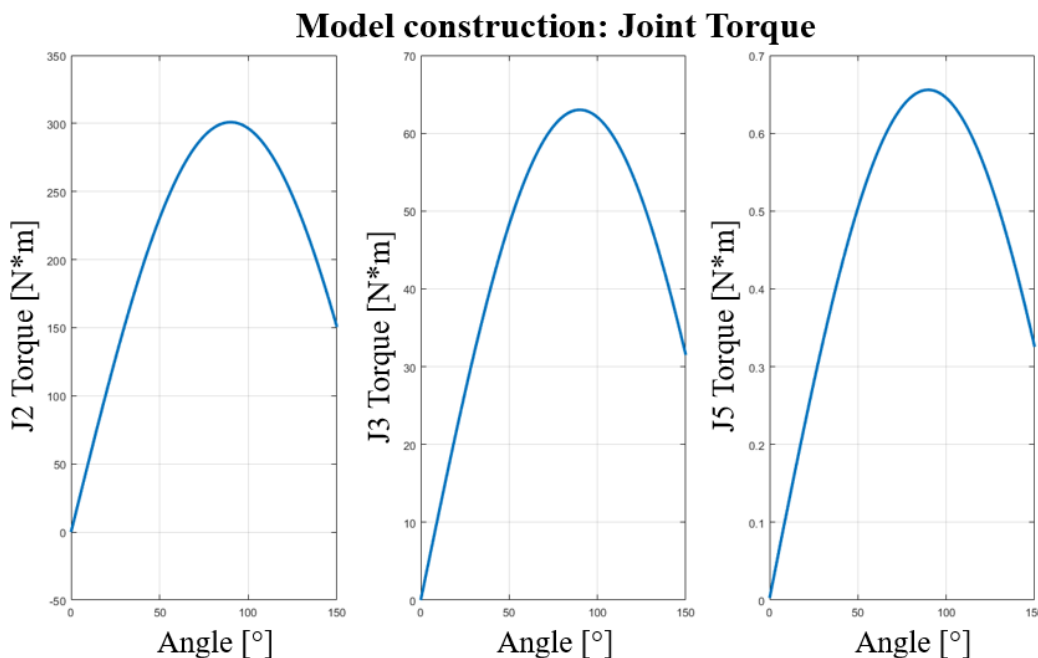
Figure 9 Model construction – Joint 2, Joint 3, Joint 5 Torque

The torques measured on Joint 1, Joint 4, and Joint 6 register as zero, a consequence of their relatively small lever arms in relation to which the torque is computed. Here, the lever arm refers to the distance between the axis of rotation of the joint and the *Center of Mass* of the reference part.

Conversely, the torque observed on Joint 2, Joint 3, and Joint 5 exhibits an increase proportional to the assigned angular displacement. Specifically, these values demonstrate a sinusoidal fluctuation pattern over time, becoming more pronounced as the joint's angular displacement amplifies. This phenomenon can be attributed to the lever arm, around which the torque is calculated, expanding from 0° to 90°, reaching its apex at 90°. Subsequently,

18

it gradually diminishes, reaching zero at 180°, and achieves its maximum negative value at 270°. Following this, the lever arm once again begins to rise, eventually returning to its initial position at 0°.

2.4.2 Creation of the *End Effector* temporal position measurement

Similarly, it is useful to define a measurement of the temporal position assumed by the *End Effector*, so that the trajectory it follows during the cobot's movements can be examined.

The trajectory traced by the *End Effector* during the experimental simulation is automatically generated by the *DART Studio* platform.
Particularly, this interface facilitates exporting simulation results in a file format that includes columns of various experimental parameters, such as the *End Effector*'s position and orientation, indicated respectively as 'Task Position' and 'Task Orientation'.

Conversely, The Adams Post Processor does not provide the position of the End Effector among its output variables.
Hence, to extract the trajectory described by the *End Effector* in the numerical environment, it is necessary to create the corresponding measurement within the *Adams View* software.
The workflow for determining the temporal position of the *End Effector* is very easy: simply create a marker at its upper end, labeled as *m_TaskPos* in the multibody model. Subsequently, using Adams' Post Processor, it is possible to evaluate the 'Translational_Displacement' associated with the created marker.

The Doosan H2515 datasheet provides both the coordinates of the *End Effector*'s *Center of Mass* and the height of each part of the cobot along the Z-axis (vertical axis). Utilizing these values allows the derivation of *m_TaskPos* coordinates:

- *X* coordinate: *x* coordinate of the *End Effector*'s *Center of Mass*;
- *Y* coordinate: *y* coordinate of *End Effector*'s *Center of Mass*;
- *Z* coordinate: overall height of the cobot along Z-axis.

2.4.3 Creation of the *End Effector* acceleration measurement

To compute the acceleration of the *End Effector* in the numerical environment, a method akin to that used for determining the position is employed, as outlined in Paragraph 2.4.3.

In the numerical environment, using the created marker 'm_TaskPos', the 'Translational_Acceleration' associated with the marker was extracted from the *Adams View* Post Processor.

On the contrary, experimental simulation does not directly provide the values of acceleration over time.

Therefore, this quantity was computed in the MATLAB environment using the forward difference method. Specifically, acceleration is obtained as the ratio between the differences of adjacent elements of the velocity vector and the adjacent differences of the vector of time instances.

It is important to note that the method employed to evaluate experimental acceleration computes approximate derivatives. Consequently, despite data interpolation being conducted, the experimental acceleration curve exhibits a non-continuous trend.

Chapter 3

Validation of the cobot's statics

In this chapter, the validation process of the cobot's static behavior will be thoroughly conducted. This entails establishing reference configurations specifically tailored for static analysis, followed by the measurement of torques exerted on the joints essential for maintaining the cobot in stationary positions.

Static validation ensures that the robot can properly perform its intended functions without moving or deforming undesirably when subjected to external stresses.

Finally, the joint torque values obtained from both experimental and numerical simulations are compared and analyzed in relation to the corresponding values derived from the analytical calculation of static torques.

3.1 Definition of reference configurations for static analysis

To validate the cobot's static behavior, it is essential to calculate the torque exerted by each joint at specific positions of the system. These positions serve as the reference configurations for analyzing the robot's statics. Therefore, simulations in both experimental and numerical environments will be conducted based on these configurations. Furthermore, they are also utilized as the reference for performing analytical calculations.

The defined reference configurations are as follows:

1. Reference static configuration for Joint 2: all joints are set to 0°, except Joint 2, which is positioned from 15° to 90° in increments of 15°.

   For Joint 2, the reference configurations are set from 0° to 90°, unlike the other two joints considered which range from 0° to 135°. This adjustment is necessary due to the

experimental setup of the physical robot in the laboratory, where tilting it beyond 90° would result in collision with the worktable.

In essence, the robot's relative positioning to the worktable restricts the movement of Joint 2 beyond 90°.

Figure 10 shows an example of the reference configuration for Joint 2 positioned at 45°:

Figure 10 Static configuration of Joint 2 at 45°

2. Reference static configuration for Joint 3: all joints are set to 0°, except Joint 3, which is positioned from 15° to 135° in increments of 15°.

Figure 11 is an example of the reference configuration for Joint 3 positioned at 45°:
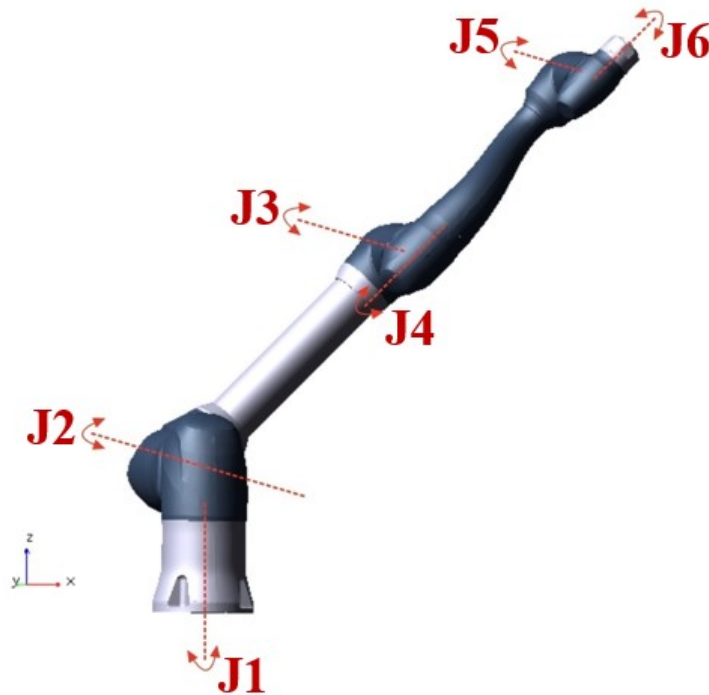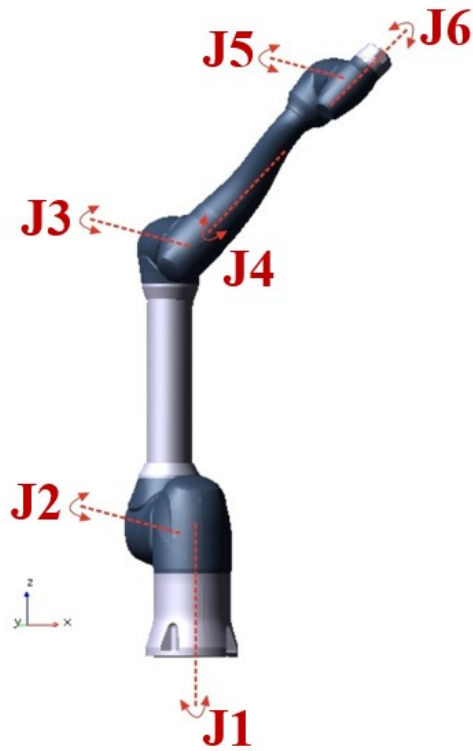
Figure 11 Static configuration of Joint 3 at 45°

3. Reference static configuration for Joint 5: all joints are set to 0°, except Joint 5, which is positioned from 15° to 135° in increments of 15°. Figure 12 Static configuration of Joint 5 at 45° is an example of the reference configuration for Joint 5 positioned at 45°:

Figure 12 Static configuration of Joint 5 at 45°

23
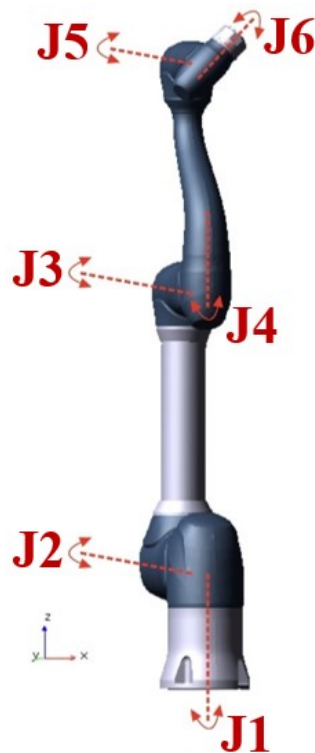
The logic behind the selection of Joints 2, 3, and 5 to define the reference configurations was described upon in the previous chapter: it was explained that due to the exceedingly minimal distance from the rotational axis of these joints to the *Centers of Mass* of the reference parts, the resulting torques are likewise minimal, or even negligible. Consequently, Joints 1, 4, and 6 would not provide particularly relevant information for examining the statics of the Doosan H2515.

3.2 Analytical computation of joint torques in static conditions

3.2.1 Analytical computation of Joint 2 Torque in static conditions

The analytical solution for calculating Joint 2 Torque in static condition is presented in this paragraph.

The primary objective of this analytical calculation is to determine the torque needed to maintain the static reference configuration:

$$Torque = Force * Distance \qquad \text{(Equation 3.1)}$$

The force can be determined through the following calculations:

$$Force = m_{TOT} * a, \text{ with } a = g = 9.81 \ m^2/s \qquad \text{(Equation 3.2)}$$

Where the total mass equals the sum of the masses of Part 2 and all components downstream of it:

$$m_{TOT} = m_2 + m_3 + m_4 + m_5 + m_6 \qquad \text{(Equation 3.3)}$$

The *Distance* is computed between the Part 2's *Center of Mass* (COM) and Joint 2's axis of rotation:

$$Distance_2 = (z_2 - d) * sin\alpha + x_2cos\alpha = [mm] \quad \text{(Equation 3.4)}$$

Where:

- α: Joint 2 angular displacement – referred to the vertical axis;

- z_2: Z-coordinate of the *Center of Mass* of Part 2;

- x_2: X-coordinate of the *Center of Mass* of Part 2;

- d: Joint 2 axis of rotation height.

- Figure 13 provides a graphical representation of the quantities used in the Equation 3.
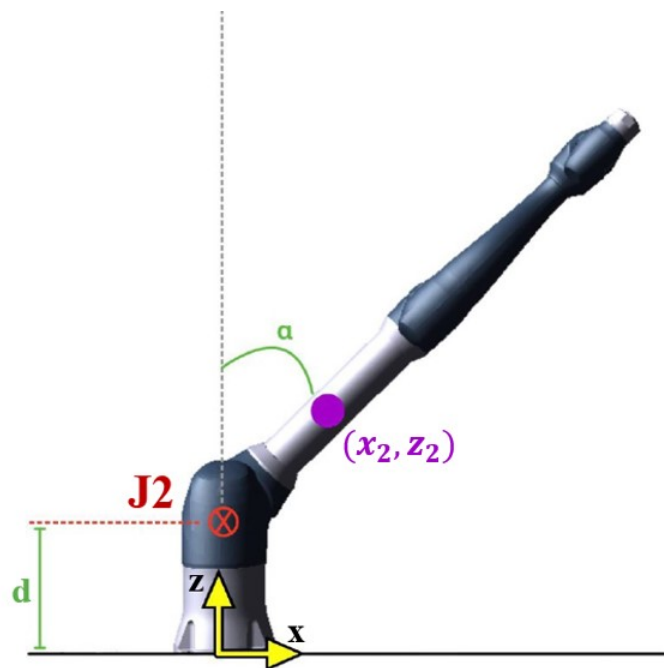
Figure 13 Analytical computation of Joint 2 Torque

As illustrated in the Equation 3.4, both the *x* and *z* components of the *Center of Mass* must be considered to calculate the *Distance*.

The same procedure is employed to compute the *Distance* of the remaining parts of the cobot from Joint 2, where the *x* and *z* coordinates in the Equation 3.4 are replaced with those of the *Center of Mass* of the specific part under consideration:

$$Distance_3 = (z_3 - d) * sin\alpha + x_3cos\alpha = [mm] \quad \text{(Equation 3.5)}$$

$$Distance_4 = (z_4 - d) * sin\alpha + x_4 cos\alpha = [mm] \qquad \text{(Equation 3.6)}$$

$$Distance_5 = (z_5 - d) * sin\alpha + x_5 cos\alpha = [mm] \qquad \text{(Equation 3.7)}$$

$$Distance_6 = (z_6 - d) * sin\alpha + x_6 cos\alpha = [mm] \qquad \text{(Equation 3.8)}$$

The total *Distance* is the mass-weighted average of the distances of each part considered:

$$Distance_{TOT} = \frac{m_2 * Distance_2 + m_3 * Distance_3 + m_4 * Distance_4 + m_5 * Distance_5 + m_6 * Distance_6}{m_{TOT}} \qquad \text{(Equation 3.9)}$$

In conclusion, the torque on Joint 2 is:

$$J2_{Torque} = \frac{Distance_{TOT}}{1000} * m_{TOT} * 9.81 = [N * m] \qquad \text{(Equation 3.10)}$$

3.2.2 Analytical computation of Joint 3 Torque in static conditions

The analytical solution for calculating Joint 3 Torque in static condition is presented in this paragraph.

The primary objective of this analytical calculation is to determine the torque needed to maintain the static reference configuration:

$$Torque = Force * Distance \qquad \text{(Equation 3.11)}$$

The force can be determined through the following calculations:

$$Force = m_{TOT} * a, \text{ with } a = g = 9.81 \ m^2/s \qquad \text{(Equation 3.12)}$$

Where the total mass equals the sum of the masses of Part 3 and all components downstream of it:

$$m_{TOT} = m_3 + m_4 + m_5 + m_6 \qquad \text{(Equation 3.13)}$$

The *Distance* is computed between the Part 3's *Center of Mass* (COM) and Joint 3's axis of rotation:

$$Distance_3 = (z_3 - d) * sin\alpha + x_3 cos\alpha = [mm] \quad \text{(Equation 3.14)}$$

Where:

- α: Joint 3 angular displacement – referred to the vertical axis;

- z_3: Z-coordinate of the *Center of Mass* of Part 3;

- x_3: X-coordinate of the *Center of Mass* of Part 3;

- d: Joint 3 axis of rotation height.

Figure 14 provides a graphical representation of the quantities used in the Equation 3.14:
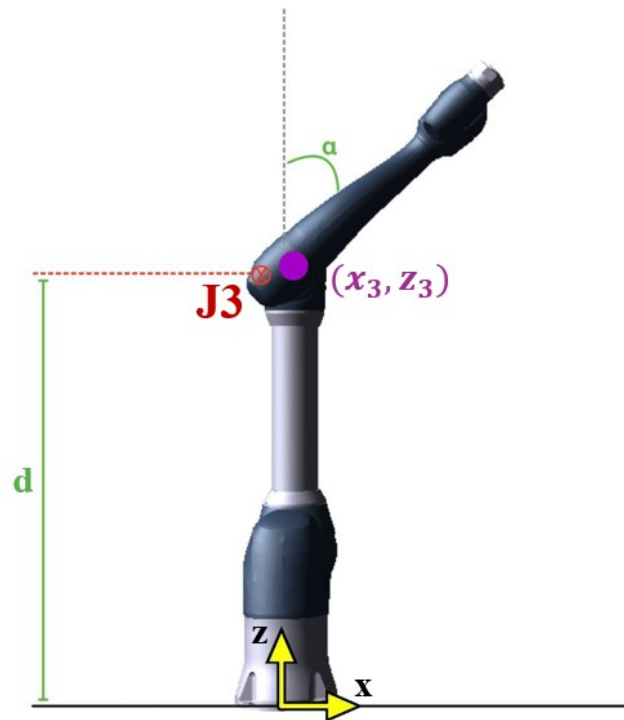
Figure 14 Analytical computation of Joint 3 Torque

As illustrated in the Equation 3.14, both the *x* and *z* components of the *Center of Mass* must be considered to calculate the *Distance*.

The same procedure is employed to compute the *Distance* of the remaining parts of the cobot from Joint 3, where the *x* and *z* coordinates in the Equation 3.14 are replaced with those of the *Center of Mass* of the specific part under consideration:

$$Distance_4 = (z_4 - d) * sin\alpha + x_4 cos\alpha = [mm] \qquad \text{(Equation 3.15)}$$

$$Distance_5 = (z_5 - d) * sin\alpha + x_5 cos\alpha = [mm] \qquad \text{(Equation 3.16)}$$

$$Distance_6 = (z_6 - d) * sin\alpha + x_6 cos\alpha = [mm] \qquad \text{(Equation 3.17)}$$

The total *Distance* is the mass-weighted average of the distances of each part considered:

$$Distance_{TOT} = \frac{m_3 * Distance_3 + m_4 * Distance_4 + m_5 * Distance_5 + m_6 * Distance_6}{m_{TOT}} \qquad \text{(Equation 3.18)}$$

In conclusion, the torque on Joint 3 is:

$$J3_{Torque} = \frac{Distance_{TOT}}{1000} * m_{TOT} * 9.81 = [N * m] \qquad \text{(Equation 3.19)}$$

3.2.3 Analytical computation of Joint 5 Torque in static conditions

The analytical solution for calculating Joint 5 Torque in static condition is presented in this paragraph.

The primary objective of this analytical calculation is to determine the torque needed to maintain the static reference configuration:

$$Torque = Force * Distance \qquad \text{(Equation 3.20)}$$

The force can be determined through the following calculations:

$$Force = m_{TOT} * a, \text{ with } a = g = 9.81 \, m^2/s \qquad \text{(Equation 3.21)}$$

Where the total mass equals the sum of the masses of Part 5 and all components downstream of it (in this scenario, Joint 5 is tasked solely with supporting the mass of Part 6, in addition to that of Part 5):

$$m_{TOT} = m_5 + m_6 \qquad \text{(Equation 3.22)}$$

The *Distance* is computed between the Part 5's *Center of Mass* (COM) and Joint 5's axis of rotation:

$$Distance_5 = (z_5 - d) * sin\alpha + x_5 cos\alpha = [mm] \quad \text{(Equation 3.23)}$$

Where:

- α: Joint 5 angular displacement – referred to the vertical axis;

- z_5: Z-coordinate of the *Center of Mass* of Part 5;

- x_5: X-coordinate of the *Center of Mass* of Part 5;

- d: Joint 5 axis of rotation height.

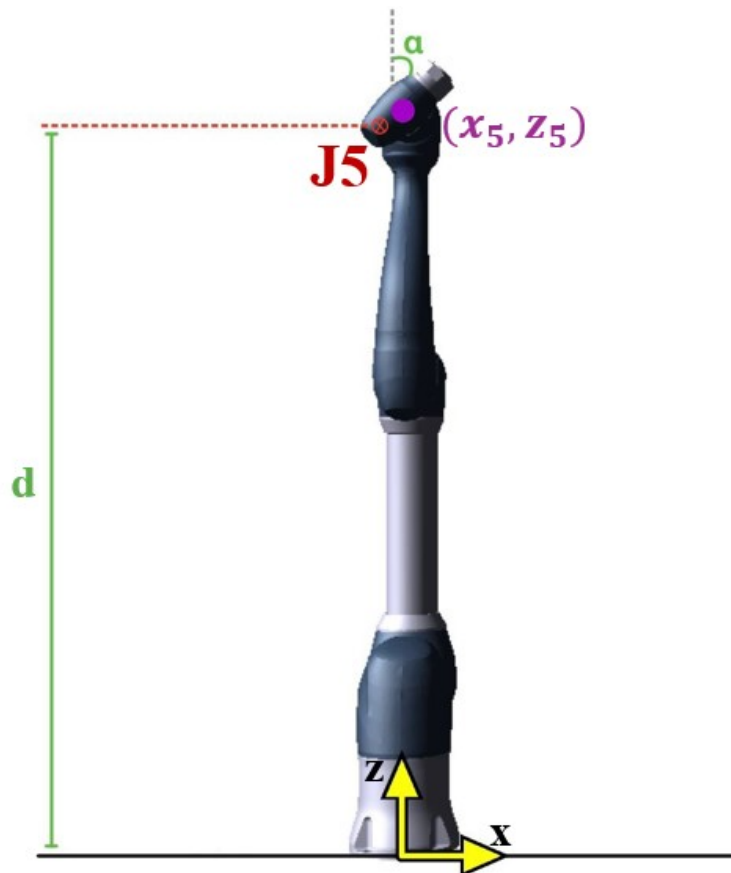Figure 15 provides a graphical representation of the quantities used in the Equation 3.23:

Figure 15 Analytical computation of Joint 5 Torque

As illustrated in the Equation 3.23, both the *x* and *z* components of the *Center of Mass* must be considered to calculate the *Distance*.

The same procedure is employed to compute the *Distance* of the remaining parts of the cobot from Joint 5, where the x and z coordinates in the Equation 3.23 are replaced with those of the *Center of Mass* of the specific part under consideration:

$$Distance_6 = (z_6 - d) * sin\alpha + x_6 cos\alpha = [mm] \qquad \text{(Equation 3.24)}$$

The total *Distance* is the mass-weighted average of the distances of each part considered:

$$Distance_{TOT} = \frac{m_5 * Distance_5 + m_6 * Distance_6}{m_{TOT}} \qquad \text{(Equation 3.25)}$$

In conclusion, the torque on Joint 5 is:

$$J5_{Torque} = \frac{Distance_{TOT}}{1000} * m_{TOT} * 9.81 = [N * m] \qquad \text{(Equation 3.26)}$$

3.3 Analysis of the cobot's statics

3.3.1 Simulation

The analysis involved positioning Joints 2, 3, and 5 in the static reference configurations described in paragraph 3.1, in order to subsequently measure the torques relative to the joint under examination in the defined conditions.
To achieve these specific configurations, a multi-step approach was adopted: initially, a kinematic simulation (lasting 3s) was executed to precisely position the robot as desired. Subsequently, a static simulation (lasting 5s) was conducted, wherein the relevant torque quantities were extracted and analyzed.

Achieving the desired positioning necessitated the implementation of a motion law; Equation 3.27 and Figure 16 show, as an example, an analytical and graphical representation of the motion law imposed on Joint 2 to bring it to the reference configuration at 15°:
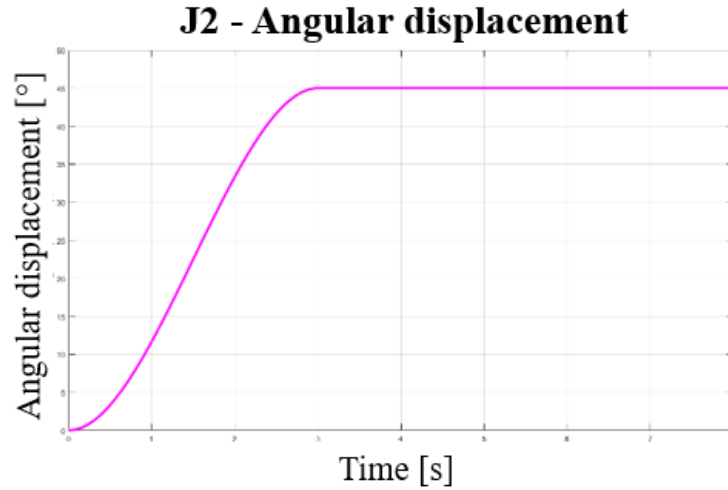
displacement(time)= step(time, 0, 0, 3, 15)

Figure 16 Validation of the cobot's statics – Joint 2 angular displacement

3.3.2 Results

The comparison between experimental *Joint Torque*, numerical *Joint Torque* and analytically calculated *Joint Torque* of Joint 3 is shown in   Figure 17:
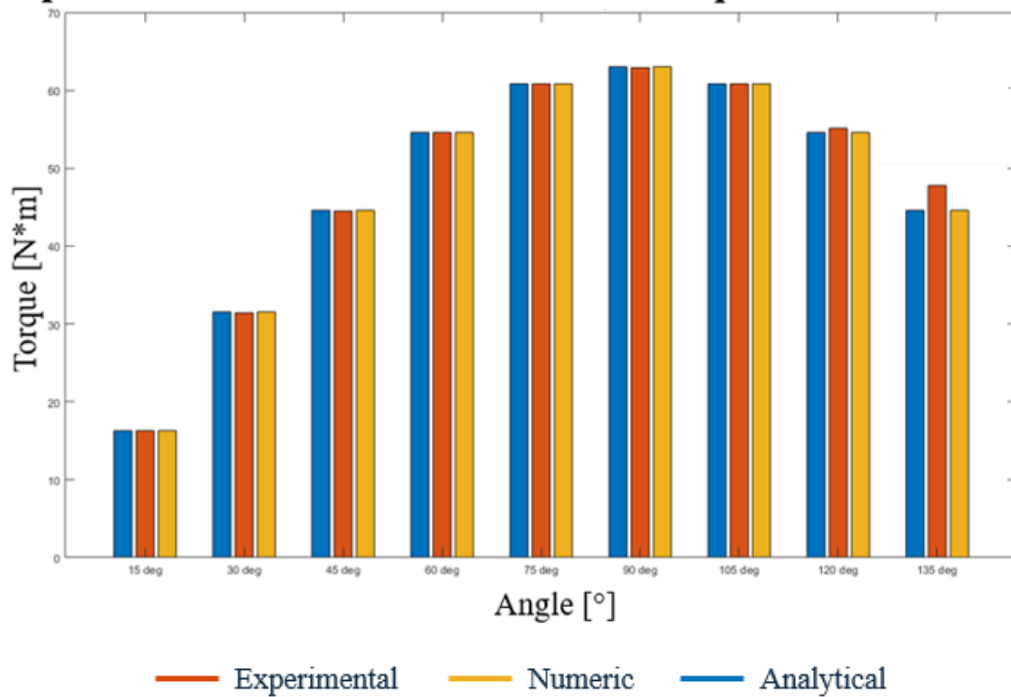

Figure 17 Comparison of the cobot's statics: Joint 3 Torque – Static Simulations

The obtained results show that the measured torques, when placing Joint 3 from 15° to 105°, can be reasonably considered closely similar. However, positioning Joint 3 at 120° and 135° yields a maximum deviation of 1% *and 7%*, respectively. These can be deemed acceptable given that the percentage error is adequately low.

In absolute terms, the maximum deviation detected is 0.594 N*m and 3.244 N*m, respectively. They can be deemed tolerable when considering the order of magnitude of *Joint Torque* – Joint 3 torque detected for an angular displacement of 120° and 135° are approximately 55 N*m and 45 N*m respectively.

In both scenarios, it is evident that the experimental outcome exceeds both the analytical and numerical results, indicating an overestimation in the former case.

The comparison between experimental *Joint Torque*, numerical *Joint Torque* and analytically calculated *Joint Torque* of Joint 5 is shown in   Figure 18:
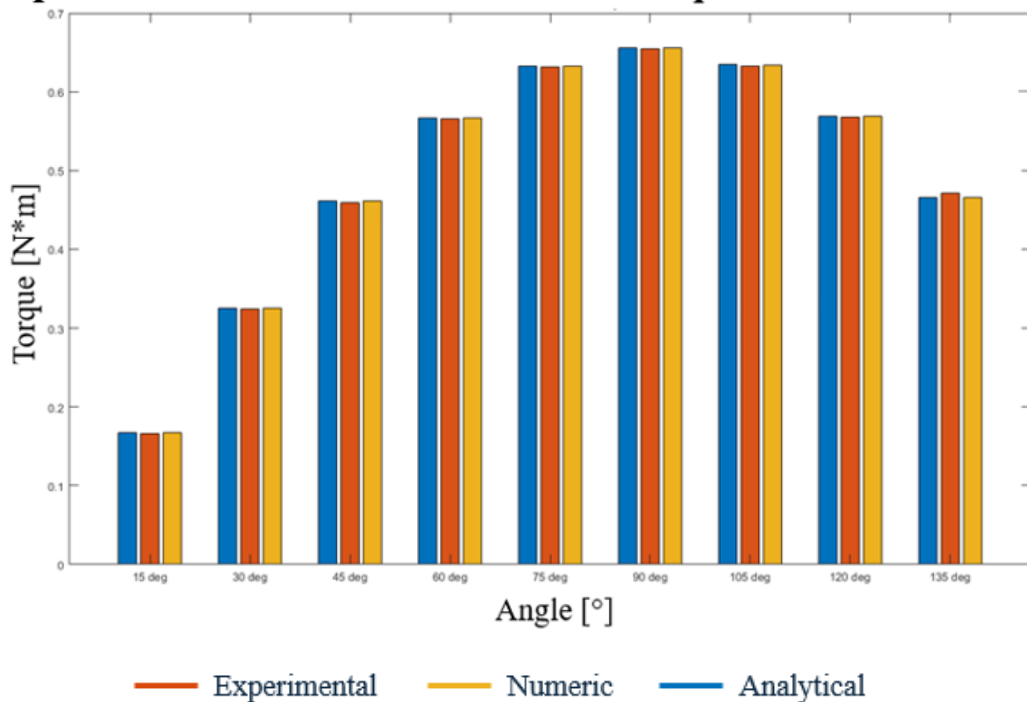

Figure 18 Comparison of the cobot's statics: Joint 5 Torque – Static Simulations

The results obtained indicate that the measured torques, when Joint 5 is positioned from 15° to 120° (excluding the configuration of 45°), can be reasonably considered nearly similar. Conversely, placing Joint 5 at 45° and 135° results in a maximum deviation -0.6% *and 1%*,

respectively. These can be deemed acceptable given that the percentage error is adequately low.

In absolute terms, the maximum deviation detected is 0.003 N*m and 0.006 N*m, respectively. They can be considered tolerable when taking into account the order of magnitude of *Joint Torque* – Joint 5 torque detected for an angular displacement of 120° and 135° are approximately 0.46 N*m and 0.47 N*m respectively.

In the first scenario, it is noted that the experimental result is lower than the analytical one, indicating an underestimation in the former case; conversely, the opposite holds true in the second scenario.

The comparison between numerical *Joint Torque* and analytically calculated *Joint Torque* of Joint 2 is shown in   Figure 19:

Figure 19 Comparison of the cobot's statics: Joint 2 Torque – Static Simulations

The analytical and numerical results exhibit good approximation across all simulated positions. However, when comparing the analytical torques with the experimental data, it becomes evident that Joint 2 is the 'critical joint' due to the significant discrepancy between the mentioned quantities.

The maximum percentage error occurs at the angle of 15° (with a deviation of -106%).

33

3.3.3 Discussion

In conclusion, the results extracted from the conducted simulations allow for the assertion that the statics of the collaborative robotic arm Doosan H2515 can be considered validated with good approximation, except for Joint 2. Indeed, this analysis highlights the critical nature of said joint.

Each joint of the cobot is equipped with a motor and a brake, and the detected criticality in the behavior of Joint 2 can be attributed precisely to the presence of these components. Specifically, the motor primarily provides the energy necessary to move the mechanical components of the device, including its parts or joints, by supplying the force needed to overcome resistance to movement and perform the designated activities of the cobot. Conversely, internal brakes serve to regulate the movement of its moving parts, allowing them to be stopped or slowed down, to maintain the robot in a stationary position, regulate the speed of its movements, or ensure safety in specific circumstances.

Although motors and brakes are integral to the actual physical system, they are not factored into the multibody model due to a lack of technical information regarding them. This consequently results in a discrepancy between experimental and numerical results, which becomes more pronounced when the cobot is tasked with movements that accentuate the action of such components.

It can be anticipated that the critical nature of this joint is not only evident in the static behavior of the system but also in its dynamic behavior, as will be elucidated in the following chapters.

Chapter 4

Validation of cobot's kinematics

This chapter serves to outline the process involved in validating the kinematics of the collaborative robotic arm, Doosan H2515.

When embarking on the kinematic validation journey for a robotic system, the overarching goal is to ensure that the real-world movements of the robot align with the predictions derived from its theoretical or numerical model.

In practical terms, the focal point lies in establishing a correspondence in the trajectory traced by the *End Effector* during the cobots movement between these two environments. Hence, an analysis is conducted to evaluate the position and orientation of this component of the system.

4.1 Implementation of the motion

The ultimate aim is to analyze the trajectory traversed by the cobot's *End Effector*, thus necessitating the initial definition and setting of the cobot's movement under examination. Contrary to commencing from its resting position, typically vertical, the system is instead brought to a predetermined starting configuration, defined by the following assigned angular displacements to the joints:

- Initial condition of Joint 1: 90°;

- Initial condition of Joint 2: 30°;

- Initial condition of Joint 3: 90°;

- Initial condition of Joint 4: 0°;

- Initial condition of Joint 5: 60°;
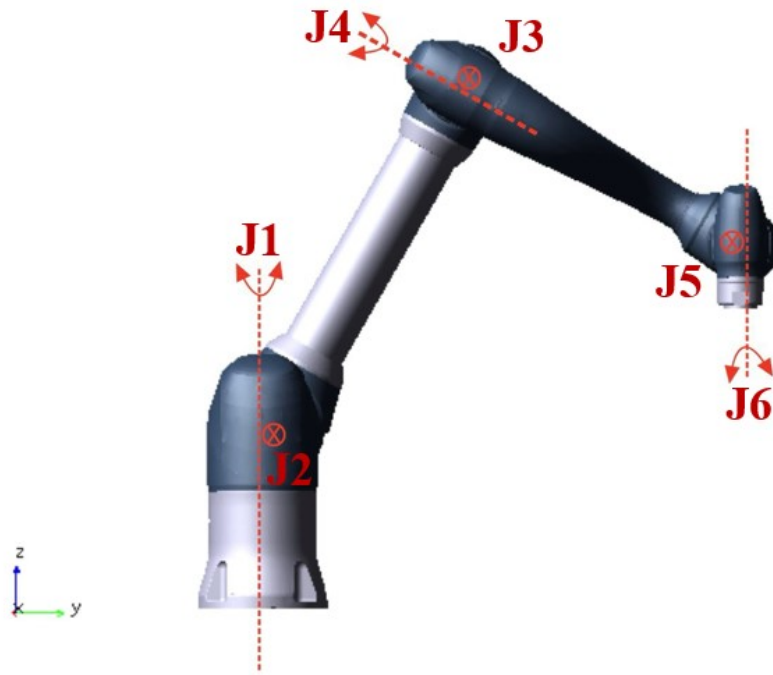
- Initial condition of Joint 6: 0°.

Figure 20 Validation of the cobot's kinematics – Starting position

Hence, to enable the cobot to reach this initial position, it is essential to allocate a specific movement to each joint, guided by the displacement law as described by Equation 2.1 in Chapter 2. In reference to this equation, the variable denoted as h_1 should be replaced with the initial displacement condition associated with each joint. Therefore, the initial movement performed by the cobot, to reach the starting position, lasts for 3s.

From this point onward, Joint 4 (denoted as "J4" in the multibody model) undergoes a 180° movement, while all other joints remain stationary – both in the experimental and numerical environments.

This movement is the one under scrutiny, in terms of the trajectory of the *End Effector*, and is configured by the following displacement law:

$$displacement(time) = 45d*(time - 3 - 1) \qquad \text{(Equation 4.1)}$$

As detailed in the Equation 4.1, the second movement occurs (3+1)s subsequent to the initiation of the simulation.

This delay is intentional and is related to the preceding explanation that the collaborative robot must first attain its initial position (through a movement lasting 3s) before commencing further actions.

36

The inclusion of "+1" in the motion law elucidates that once the initial configuration is achieved, the robot maintains a stationary state for a duration of 1s before embarking on the second movement. This deliberate pause in the robot's motion is motivated by the desire to distinctly delineate between the two movements, thereby facilitating a more focused analysis on the subsequent action. Consequently, the initial movement primarily serves the purpose of positioning the robot at a predetermined starting point, allowing for a clear and isolated examination of the subsequent motion.

4.2 Analysis of the cobot's kinematics

4.2.1 Simulation

In order to study the cobot's kinematics, the following simulations are conducted:

1. Kinematic simulation – lasting 3s: the cobot moves to its initial position;
2. Static simulation – lasting 1s: the cobot remains stationary for a 1s time interval;
3. Dynamic simulation – lasting 4s: Joint 4 undergoes a 180° movement starting from the assigned position.

To analyze the *End Effector*'s trajectory during the movement of Joint 4, attention need only be directed to the final simulation. Everything preceding it merely ensures that the motion occurs under the desired simulation conditions.

4.2.2 Results

Figure 21, Figure 22, Figure 23 display:
- The trajectories followed by the *End Effector* over time along the X, Y, Z axes;
- The trajectories followed by the *End Effector* in the XY, XZ, YZ planes;
- The trajectory followed by the *End Effector* in three-dimensional space.

It should be noted that the *End Effector* acceleration was derived as described in paragraph 2.4.2.

Comparison of the cobot's kinematics: Task Pos vs Time - Dynamic simulation

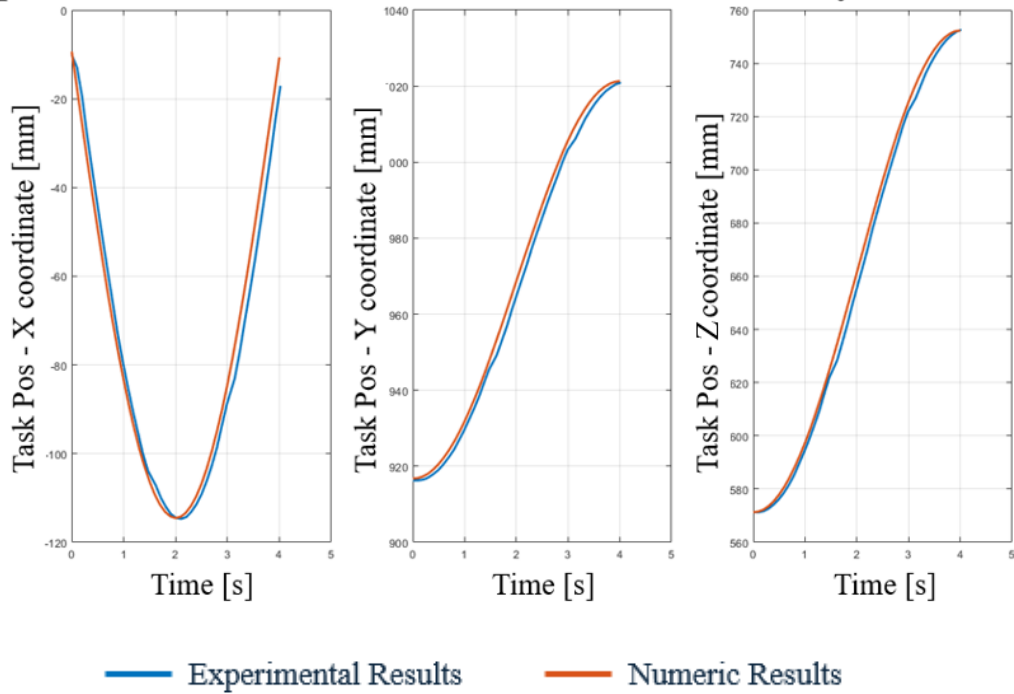*Figure 21 Comparison of the cobot's kinematics – Task Position vs Time*

Comparison of the cobot's kinematics: Task Pos - XY, XZ, YZ planes - Dynamic simulation
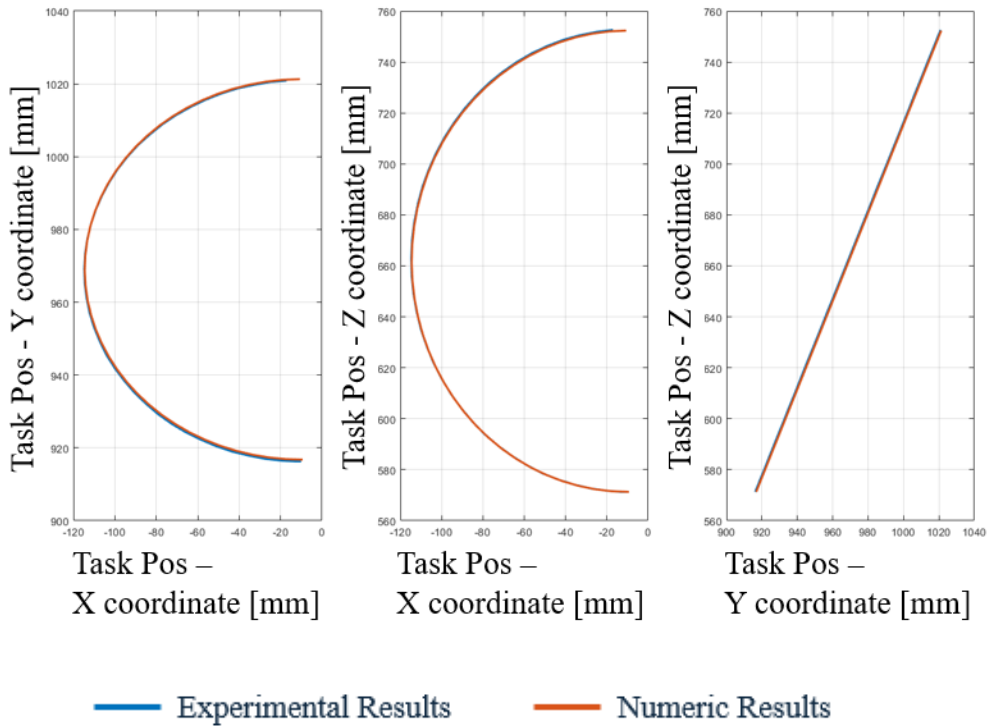

Figure 22 Comparison of cobot's kinematics – Task Position in the XY, XZ, YZ planes

Comparison of the cobot's kinematics: Task Pos - 3D space - Dynamic simulation
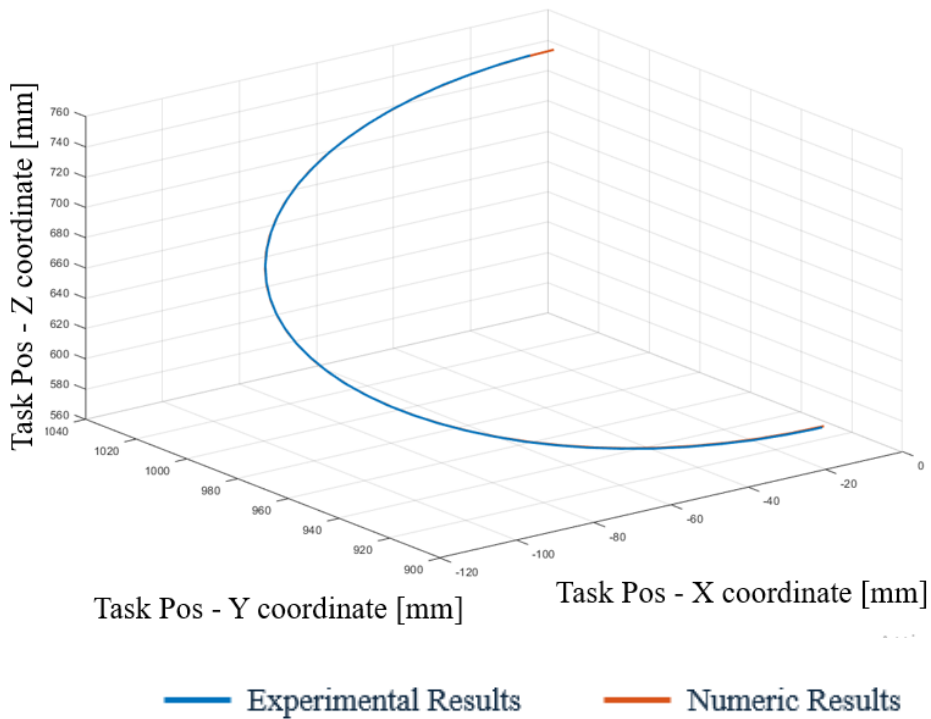
Figure 23 Comparison of the cobot's kinematics – Task Position in 3D space

In order to ultimate the validation of the cobot's kinematics, a comparison is made between experimental and numerical results regarding the acceleration of the *End Effector* during the simulated movement. It should be noted that the *End Effector* acceleration was derived as described in paragraph 2.4.3.

Figure 24 is the representation of the temporal trend of the *End Effector* acceleration along the three spatial directions:

Comparison of the cobot's kinematics: Task Acceleration vs Time - Dynamic simulation

Figure 24 Comparison of the cobot's kinematics – Task Acceleration vs Time

It is important to note that the method employed to evaluate experimental acceleration computes approximate derivatives. Consequently, despite data interpolation being conducted, the experimental acceleration curve exhibits a non-continuous trend.

4.2.3 Discussion

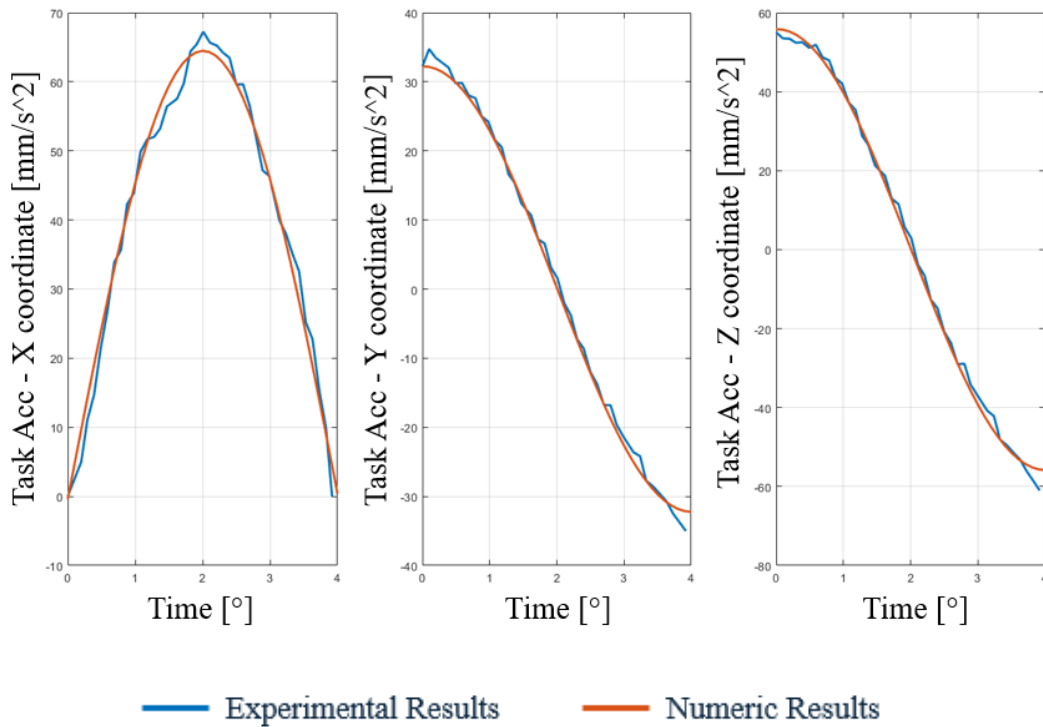To determine the validation status of the cobot's kinematics, the Root Mean Square Error is computed for both the position and the acceleration assumed by the *End Effector* in the analyzed setup.

Using RMSE in data analysis allows for quantifying the difference between the values predicted by the numerical model and the values observed experimentally and is a crucial step to determine if the validation has been successfully completed.

The curves representing the trajectory traveled by the *End Effector* over time along the three spatial directions (Figure 21) exhibit a Root Mean Square Error (RMSE) equal to:

- Root Mean Square Error along the X-direction: 4.35 mm;

- Root Mean Square Error along the Y-direction: 2.54 mm;

- Root Mean Square Error along the Z-direction: 3.58 mm.

The Root Mean Square Error (RMSE) observed between the accelerations of the *End Effector* along the three spatial directions (Figure 24) is as follows:

- Root Mean Square Error along the X-direction: 6.26 mm/s^2;

- Root Mean Square Error along the Y-direction: 2.90 mm/s^2;

- Root Mean Square Error along the Z-direction: 4.91 mm/s^2.

Upon thorough analysis and subsequent calculations, it becomes apparent that the examination conducted between the experimental and numerical representations of the *End Effector*'s position and acceleration during the simulated motion unveils a notable semblance.

It is pertinent to emphasize that the intermittent pattern observed in the experimental acceleration curve arises from the methodology employed in its computation. Unlike its numerical counterpart, this data point is not directly derived from the simulation output. Nonetheless, it closely mirrors the trajectory of the corresponding experimental curve, traversing a range of values that closely aligns with its counterpart.

Moreover, the RMSE computed between the numerical and experimental datasets relative to the *End Effector* position and acceleration across all three spatial axes falls well within the established tolerance thresholds.

In light of these considerations, there exist abundant justifications to affirm that the validation of the cobot's kinematics has been successfully established.

Chapter 5

Simulating the cobot's motion from a non-standard position

After studying and validating the static and kinematic behaviors of the Doosan H2515 cobot, attention turns to executing specific movements and applying external forces, with a clear objective: to monitor and analyze how the robotic arm joints respond to commands to start or stop motion.

Chapter 5 delves into examining the cobot's behavior during movements that do not start from its default vertical position. The data and insights gathered from this analysis are instrumental in comparing this simulation condition with that analyzed in *Chapter 6*: the cobot's movement when starting from its resting or default position.

The goal is to ensure that the cobot can reliably perform its tasks, regardless of its initial configuration, and to validate that the model accurately represents its real-world behavior under varying circumstances.

5.1 Implementation and simulation of the motion from a non-standard position

The movement to be analyzed in this chapter is exactly as described in paragraph 4.1.

Figure 25 and Figure 26 depict respectively the initial and final positions of the cobot relative to this movement:

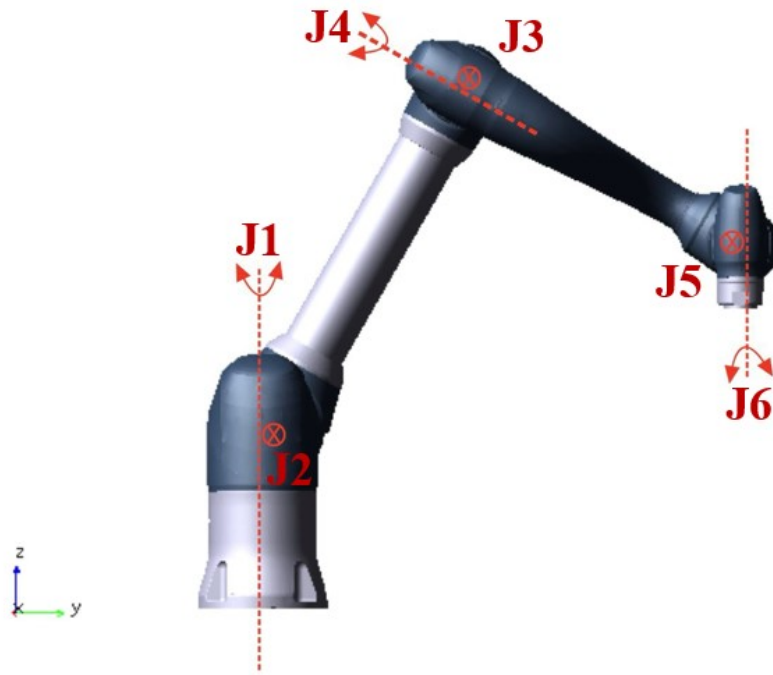*Figure 25 Cobot's motion from a non standard position – Starting configuration*
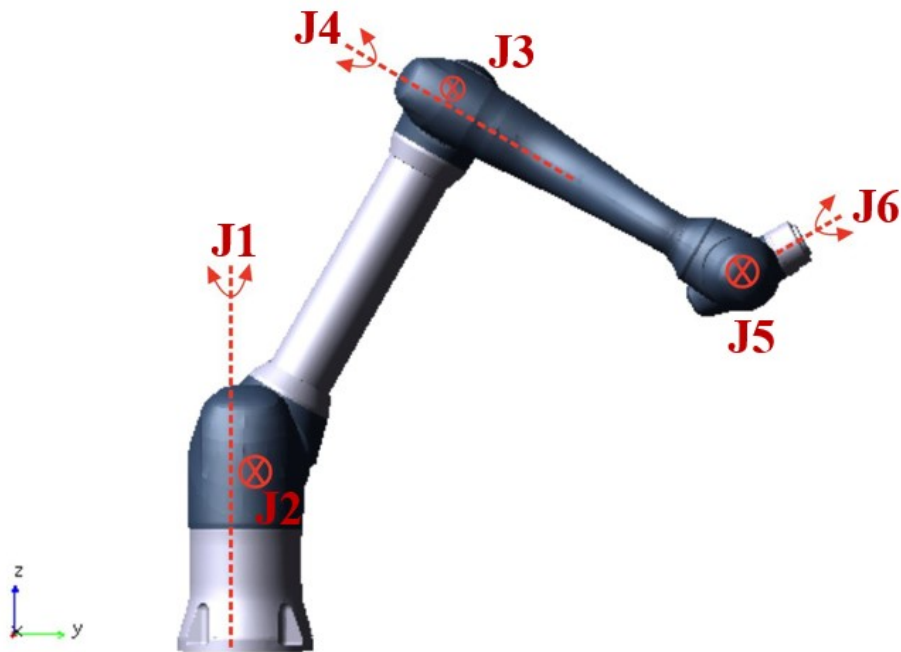

Figure 26 Cobot's motion from a non standard position – Final configuration

In order to study Joint 4 180° motion, the following simulations are conducted:

1. Kinematic simulation – lasting 3s: the cobot moves to its initial position;

2. Static simulation – lasting 1s: the cobot remains stationary for a 1s time interval;

3. Dynamic simulation – lasting 4s: Joint 4 undergoes a 180° movement starting from the assigned position.

It should be noted that in this scenario attention need only be directed to the final simulation. Everything preceding it merely ensures that the motion occurs under the desired simulation conditions.

5.2 Results of the analysis of the motion from a non-standard position

Comparing the torques measured on the joints in the two simulation environments, results shown in Figure 27 are extracted:

Cobot's motion from a non-standard position: Joint Torque - Dynamic simulation
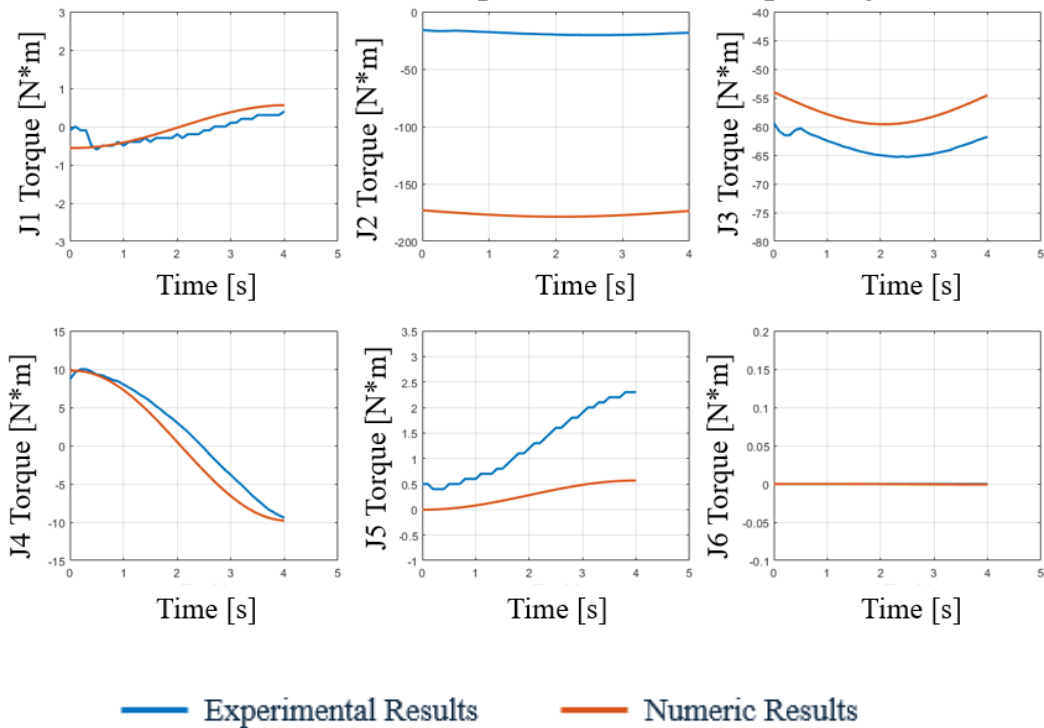
Figure 27 Cobot's motion from a non standard position – Joint Torques – Dynamic simulation

For each joint, there is an observable deviation between the experimental and numerical results. This stems from the moment the cobot deviates from its standard vertical position, triggering the engagement of its motors and brakes.

Each joint of the cobot is equipped with a motor and a brake, but although motors and brakes are integral to the actual physical system, they are not factored into the multibody model due to a lack of technical information regarding them. This consequently results in a discrepancy between experimental and numerical results, which becomes more pronounced when the cobot is tasked with movements that accentuate the action of such components – for example, a movement that does not start from the vertical position. In this case, each joint must exert a torque that is necessary not only to perform the desired movement but also to maintain the desired position during that movement. Thus, the action of the respective motors and brakes is accentuated in such cases.

Furthermore, as mentioned in Chapter 3, the critical nature of Joint 2 is evident, where the discrepancy between the results obtained is enormously pronounced.

Chapter 6

Simulating the cobot's motion from the standard position

The main objective is to monitor and analyze how the robotic arm's joints respond to commands to start or stop movement. It has been observed that if the cobot performs a movement starting from a position different from its resting position, the absence of the motors and brakes components in the system's six joints becomes evident by observing the discrepancy between the Joint Torques measured experimentally and numerically, as described in *Chapter 5*. Therefore, *Chapter 6* aims to analyze the behavior exhibited by the cobot when the initial configuration of the movement is the standard one (vertical position of the robotic arm).

In accordance with the considerations made, the expected result is that in this simulation condition, no gap (or at least very small gap) will be observed between the quantities of interest – precisely because the action exerted by the motors and brakes is much less pronounced.

6.1 Implementation of the motion from the standard position

Starting from the vertical configuration, Joint 3 (designated as "J3" in the multibody model) undergoes a 135° movement, while all other joints remain stationary – both in the experimental and numerical environments.
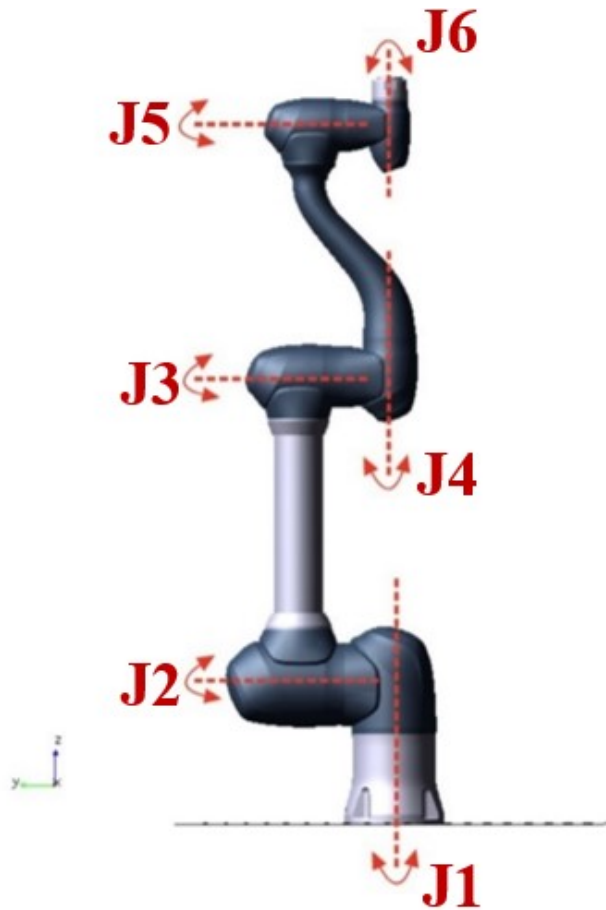
Figure 28 Doosan H2515 vertical configuration

Joint 3 moves at a constant speed of 5 °/s, taking 27s to complete the angular displacement of 135°. Consequently, the simulation runs for a duration of 27s.

It becomes apparent, however, that the cobot cannot immediately achieve a constant velocity. Initially, starting from a stationary position, it gradually accelerates, facilitating the eventual attainment of a velocity of 5°/s. This acceleration process allows the cobot to smoothly transition to and maintain the desired velocity consistently throughout the movement.

Likewise, as the movement draws to a close, Joint 3 continues to move at a steady velocity until just before the conclusion of the simulation, where a slight deceleration occurs, leading to a gradual halt.

Specifically, the cobot undergoes an initial acceleration and a final deceleration of $0.2°/s^2$. This observed behavior is not only replicated faithfully in the numerical simulation but also consistently observed in the experimental environment.

At the conclusion of the described motion, the cobot reaches the position shown in Figure 29:
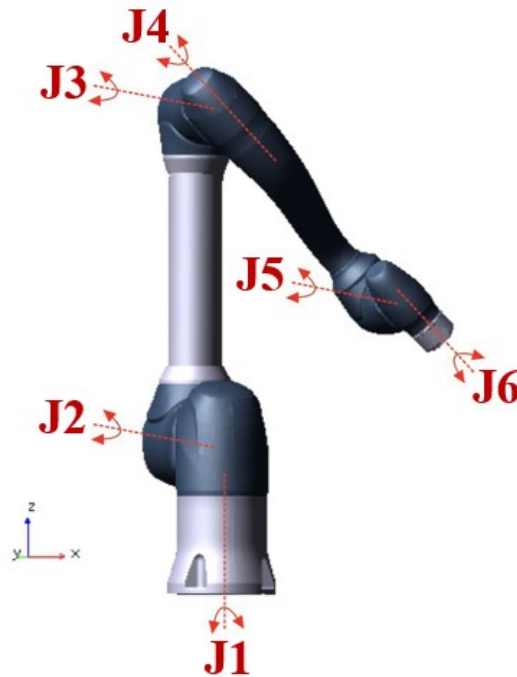

Figure 29 Cobot's motion from the standard position – Final configuration

The angle formed by Joint 3 with the vertical is indeed 135°.

In the current scenario, the motion is defined by assigning a velocity law, which inherently incorporates the ability to model acceleration. Conversely, in the previous chapter, a displacement law was utilized, implicitly assuming constant displacement from the simulation's outset.

So, to ensure consistent behavior of the cobot in the *Adams View* environment, the motion law described in Equation 6.1 must be assigned to Joint 3:

$$velocity(time) = step(time, 0, 0, 0.2, 5) – step(time, 26.8, 0, 27, 5) \quad \text{(Equation 6.1)}$$

It should be noted that Equation 6.1 has the same structure as Equation 2.1, with the only difference being that the dependent variable is velocity rather than displacement.

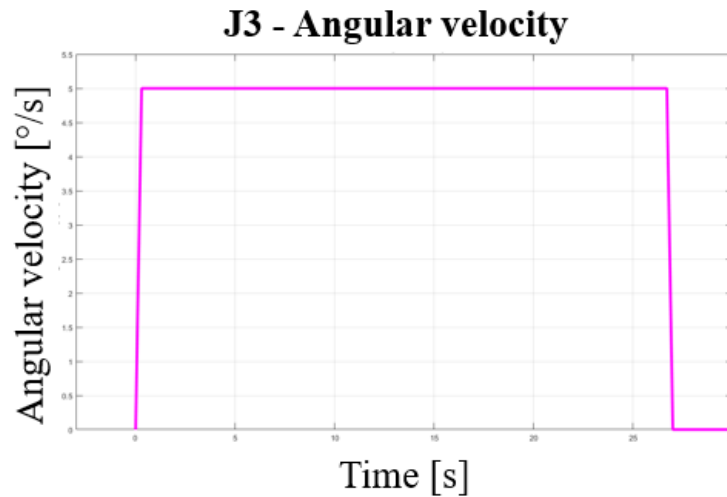Figure 30 is the representation of this motion law:

Figure 30 Cobot's motion from the standard position – Joint 3 angular velocity

The motion assignment through a velocity law and the disparity between the two step functions effectively reproduce the initial acceleration and final deceleration experienced by the robotic arm.

To keep the remaining joints stationary, a motion of 0° lasting for 27s must be imposed on them.

6.2 Results of the analysis of the cobot's motion from the standard position

In both the experimental and numerical environments, a dynamic simulation lasting 27s is carried out.

Subsequently, the post-processing phase involves the measurement of the torque experienced by each joint throughout the simulation duration. Figure 31 shows the comparative analysis of the Joint Torque data obtained from both experimental and numerical settings:

Cobot's motion from the standard position: Joint Torque - Dynamic simulation
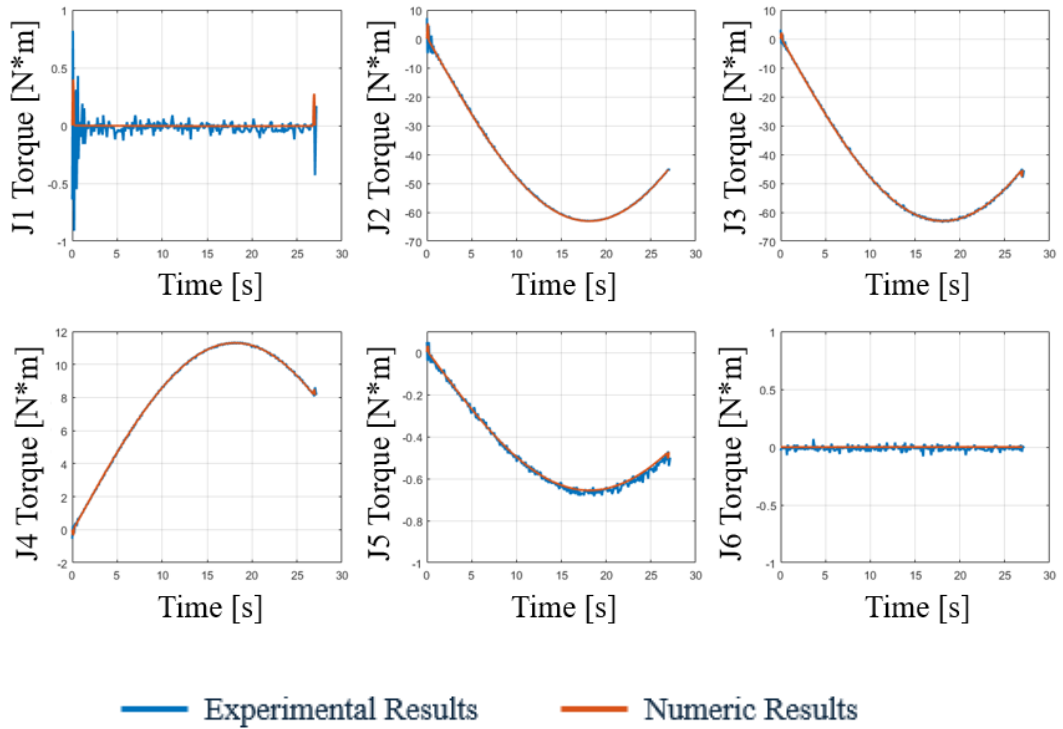
Figure 31 Cobot's motion from the standard position – Joint Torques

The obtained results indicate that the Experimental *Joint Torque* curves closely overlap with the Numeric *Joint Torque* Curves – as it was predicter before starting this analysis.

Furthermore, a slight peak can be observed at the beginning and end of the curves, which is easily noticeable in the results of Joint 3 and Joint 4. Figure 32 and Figure 33 are an example of Joint 3:

Cobot's motion from the standard position: Joint 3 Numeric Torque
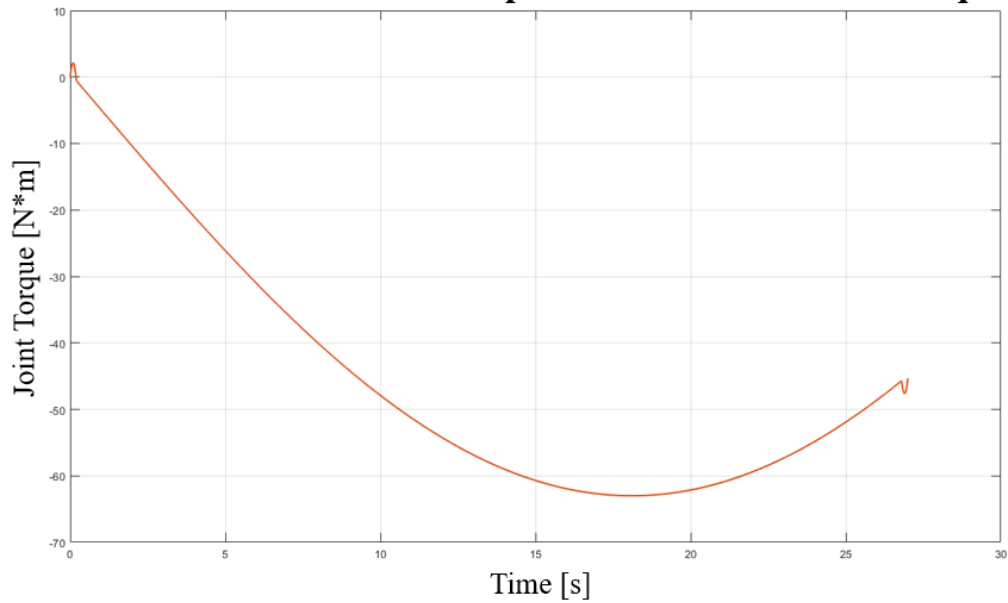

Figure 32 Cobot's motion from the standard position – Joint 3 Numeric Torque

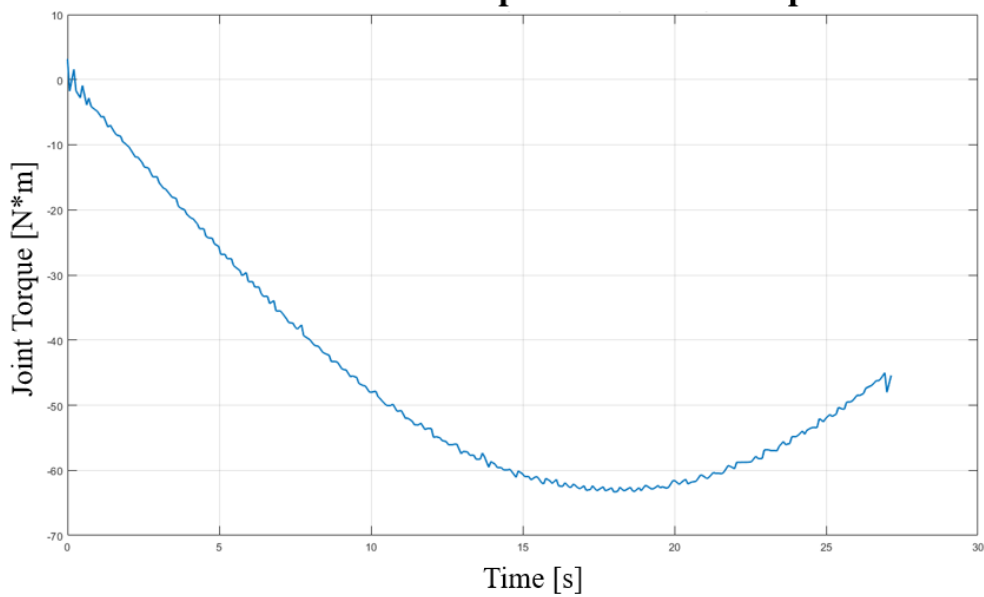**Cobot's motion from the standard position: Joint 3 Experimental Torque**

Figure 33 Cobot's motion from the standard position – Joint 3 Experimental Torque

This is attributed to the initial acceleration and final deceleration required to achieve a constant speed of 5°/s and bring the cobot to a stop.

By observing the torque trends detected on each of the cobot's joints and subsequently comparing the values extracted from both the numerical and experimental simulations, it becomes evident that the curves are almost equivalent with excellent approximation. This observation allows for the confident affirmation of the accurate implementation and validation of the Doosan H2515 robotic arm's multibody model with respect to the simulated motion.

Taking all factors into consideration, there are compelling reasons to assert that if the cobot's motion commences from the default (vertical) position, the joint torque curves align almost perfectly. Conversely, when the initial position is dictated by specific initial conditions, the joint torque curves do not perfectly overlap.
The reason for the highlighted result is described in Chapter 5.

Chapter 7

Simulating the application of a constant external force

Continuing the analysis process aimed at monitoring and analyzing how the robotic arm joints respond to commands to start or stop movement, this chapter focuses specifically on exploring the cobot's response to the application of a constant external force.

By examining the cobot's response to external forces in various scenarios, valuable insights can be gained that inform and enhance the development of medical procedures and devices. In the context of potential biomedical applications for the cobot, this analysis indeed holds significant value. For instance, it could be instrumental in evaluating the force to be applied to the spine during a surgical procedure aimed at fixing a prosthetic element.

7.1 Description of the simulation environment

The application of the external force is not tied to the robot's resting position; hence, the initial step of the analysis involves positioning the cobot at the specific starting configuration, defined by the following assigned angular displacement to the joints:

- Initial condition of Joint 1: 74.4°;
- Initial condition of Joint 2: 67.8°;
- Initial condition of Joint 3: 86.6°;
- Initial condition of Joint 4: 75.9°;
- Initial condition of Joint 5: -83.3°;
- Initial condition of Joint 6: -24.8°.

Figure 34 and Figure 35 show the initial configuration of the simulation respectively from a side view an from a rear view:
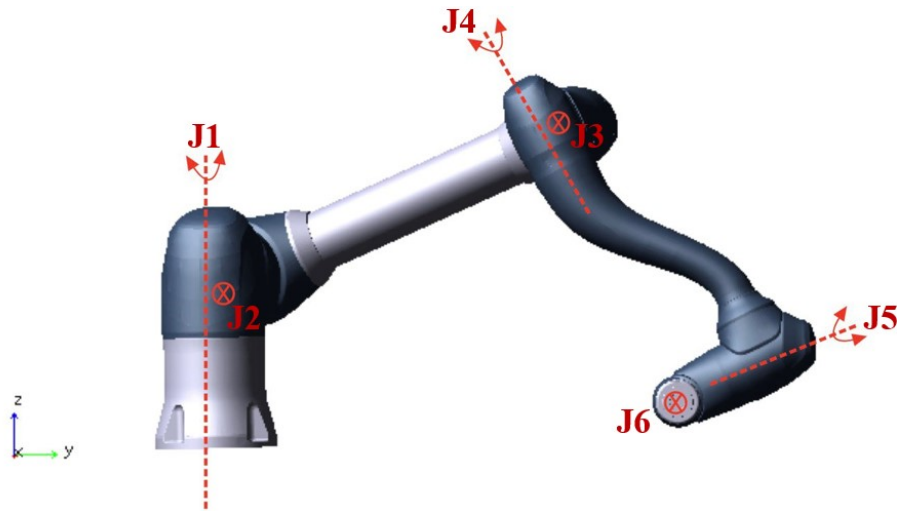
Figure 34 Application of a constant external force – Cobot configuration – Side view
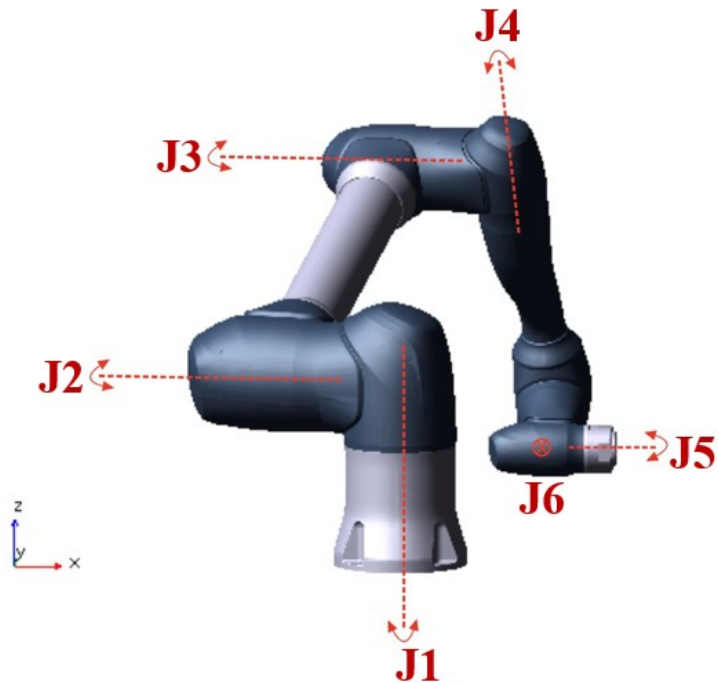
Figure 35 Application of a constant external force – Cobot configuration – Rear view

Commencing from this configuration, a constant external force is created and applied to the *End Effector* (identified as "Part 6" in the multibody model) while the cobot maintains its stationary position – across both the numerical and experimental environments.

The external force acts along the negative X-axis and has a costant magnitude of 50 N.

This configuration is modeled both in a numerical environment and in an experimental environment.

More specifically, in the experimental environment, a wall (Figure 36) is used to help reproduce the application of the external force:
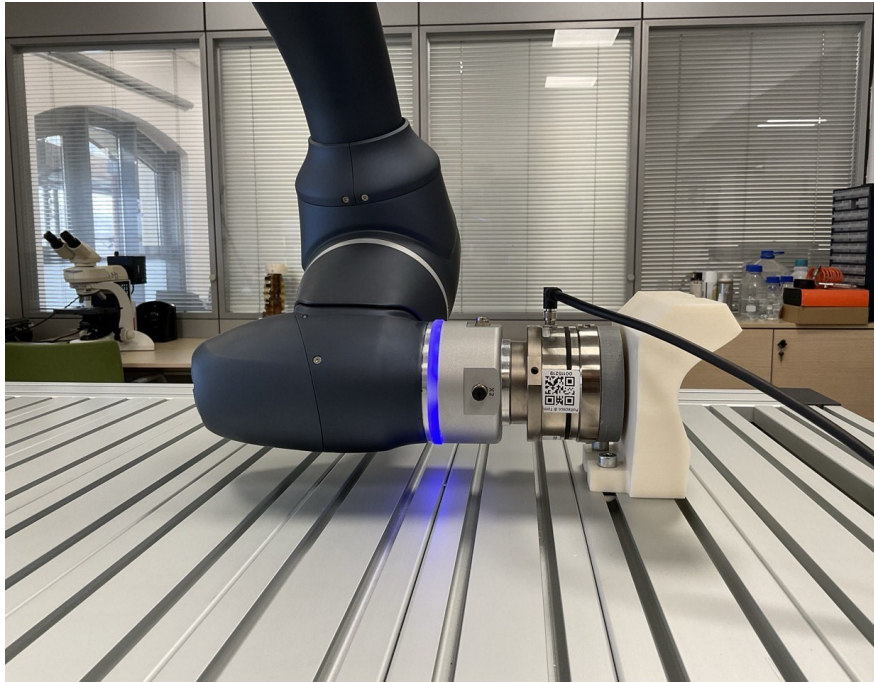
Figure 36 Experimental application of a constant external force

7.2 Implementation of the simulation environment

Initially, the cobot needs to be positioned at the specified initial point, necessitating the establishment of six motion laws, each corresponding to a joint. Specifically, each joint is assigned a displacement law as described by Equation 2.1 in Chapter 2. In reference to this equation, the variable denoted as h_1 should be replaced with the initial displacement condition associated with each joint. Hence, the initial motion executed by the cobot to reach the starting position spans a duration of 4s.

This ensures that the application of the external force can be simulated from the desired position.

As an illustration, the motion law representation for Joint 1 is provided in   Figure 37:

Figure 37 Application of a constant external force – Joint 1 angular displacement

Subsequently, a constant external force must be generated.

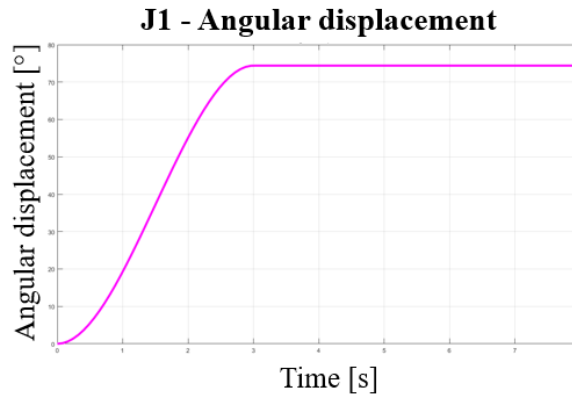The procedure for applying the force is extremely simple: it is noteworthy that the *Adams View* software provides a feature specifically designed for simulating different force applications. Within this suite of options, users can access the 'Single Component Applied Force' tool, which enables the creation of force vectors characterized by a single component with a consistent magnitude. To utilize this functionality, it is simply need to input both the desired force value and its corresponding direction within the spatial environment.

In this case, the external force is directed along the negative X-axis and maintains a constant magnitude of 50 N.

7.3 Analysis of the simulation environment

In order to investigate the mechanical response of the cobot to external forces, a series of simulations are executed as follows:

1. Kinematic Simulation – lasting 4s: during this phase, the cobot undergoes a transition to its initial configuration;

2. Static Simulation – lasting 4s: following the kinematic phase, the cobot is held stationary for a period of 4s;

3. Extended Static Simulation – lasting 10s: in this stage, the cobot is subjected to the application of a constant external force while maintaining its stationary position. This simulation enables an examination of the cobot's response to sustained external loads over an extended duration.

Given the main goal of analyzing the cobot's behavior and mechanical properties under the action of external forces, particular attention is focused on the second static simulation. In Figure 38, key parameters of interest, including experimental and numerical torque readings across the joints, are extracted and analyzed:

Figure 38 Application of a constant external force – Joint Torques – Static simulation

Table 3 shows the discrepancy measured between the experimental and numerical results when the cobot is in the assigned position, considering both the presence and absence of the external force:

Table 3 Application of a constant external force: results deviation

JOINT #	RESULTS DEVIATION [N*m] – external force applied	RESULTS DEVIATION [N*m] – no external force applied
#1	-2.66	-0.2
#2	94.53	78.49
#3	-5.09	-0.2
#4	-0.3	-0.2
#5	-1.13	-0.01
#6	0.3	0

7.4 Results of simulating the application of a constant external force

After carefully considering all the results obtained, it becomes evident that there are compelling justifications to assert that, from the static simulation incorporating the application of force significant deviations in key results are observed compared to those arising from simulations that do not account for the presence of force.

This observed deviation can be attributed to the presence of brakes within the cobot, which are not considered in the multibody model. Internal brakes play an indispensable role in controlling the movement of movable parts, ensuring they can be effectively stopped or decelerated when necessary.

In more detail, in the absence of external force application, the motor is solely tasked with maintaining the assigned position. In this scenario, experimental and numerical results align, as could be expected based on the validation of the cobot's static behavior – *Chapter 3*. Conversely, when the presence of force is considered, the discrepancy between torques increases as the motor must also counteract the influence of this external force. Consequently, this suggests that the greater the task assigned to this component, the greater the deviation between the obtained results.

However, the observed variation can still be considered acceptable when compared with the magnitude order of joint torques, except for Joint 2 ('critical joint'). Furthermore, this criticality becomes increasingly apparent as this element is further displaced from the vertical position. Indeed, in the current simulation, Joint 2 is inclined by approximately 67°, and it is noteworthy that the results deviation, although significant, decreases when the presence of external force is not considered, compared to when it is considered.

Chapter 8

Joint 2 behavior in the Doosan H2515 collaborative robotic arm

After conducting detailed simulations and analyses on the behavior exhibited by the collaborative robotic arm Doosan H2515 in various scenarios, it becomes increasingly evident that there are critical issues warranting attention, particularly concerning the absence in the numerical model of two components that are part of the real system: motors and brakes. These components were not reproduced in the numerical environment due to a lack of technical information, resulting in a discrepancy between numerical and experimental results (more or less pronounced depending on the nature and complexity of the simulations conducted).

It is important to note that what has been highlighted has implications for all joints of the system, but is particularly noticeable for those located in the central part, namely Joints 2, 3, and 4. This is justified by the fact that being very close to the base, they must also support the weight of downstream components.

More specifically, significant ambiguities have been observed, particularly in the static and dynamic behavior of Joint 2, which is indeed identified as the 'critical joint'. For this reason, attention is primarily focused on this component.

Therefore, to implement and validate the multibody model as a digital twin of the Doosan H2515 robotic arm, it is essential to understand how the actions of these components contribute to the discrepancies observed between numerical and experimental results. In particular, since the numerical method serves as the reference, the goal is to determine how the actions of these components influence the torque measured experimentally at Joint 2.

8.1 Causal Connection Between the Robotic Arm's Structure and the Critical Importance of Joint 2

All joints of Doosan H2515 are equipped with both a motor and a brake.

Motors are crucial for the robot's motion, with each joint typically featuring a dedicated motor, often a servo motor[3], enabling precise control of movement. In the case of the Doosan H2515, brushless servo motors[4] are utilized to ensure not only high precision but also energy efficiency and longevity. Specifically, the primary function of the motor in a robot is to generate the energy required to move its various mechanical components, such as joints and parts, overcoming any resistance to motion. This is achieved by converting electrical energy or other forms of energy into kinetic energy [7] [17].

Brakes are equally vital, especially for safety purposes. In robots like the Doosan H2515, they play a critical role in ensuring the safety and stability of the system. In instances of power loss or emergency scenarios, brakes serve to promptly stop and maintain the robot in its current position, reducing the risk of unintended movements that could cause damage or accidents. Additionally, brakes are used to hold the robot in a stationary position and regulate the speed of its movements, ensuring smoother and safer operation [6] [25].
Brakes may be integrated within the motors themselves or installed separately on each axis of the robot. In the brushless servo motors used in Doosan robots, brakes are integrated into the motors themselves.

These components introduce ambiguity and criticality in the behavior exhibited by Joint 2 as follows: the more the joint is inclined away from the 0° condition, the more activity is required from the mentioned components, and consequently, the greater the observed discrepancy between the results obtained.
Indeed, when the critical joint is not inclined relative to vertical, the motor and brakes only need to support the joint in bearing the weight of downstream components. Conversely, when Joint 2 is given an initial displacement condition or when movement is imposed upon

---

[3] A servo motor is an electromechanical device facilitating precise control over angular position, speed, and acceleration. Typically comprising a motor coupled with a feedback sensor and a control system, it continuously adjusts the motor's position based on received control signals from the feedback sensor.

[4] A brushless servo motor, a variant of servo motor, employs a brushless DC motor (BLDC). These motors lack brushes, resulting in enhanced efficiency, durability, and reduced maintenance requirements.

it, the motor and brakes must also act to counteract the force of gravity or any external forces, ensuring that Joint 2 successfully completes the presented task.

8.2 Analysis of Joint 2 behavior in the Doosan H2515 collaborative robotic arm

Considering the scarcity of technical documentation clarifying the operational modes of the motor and brake associated with Joint 2, an analysis of the behavior exhibited by these components has been initiated.

The ultimate goal of this analysis is to understand, with the numerical method as the reference, how the actions of these components manifest in variations of the experimentally measured torque at Joint 2, or conversely, identify the factors influencing these variations. This is essential to conclude the implementation and validation of the multibody model as a digital twin of the Doosan H2515 robotic arm.

Firstly, it is necessary to formulate hypotheses regarding potential factors influencing the behavior of Joint 2 (and thus its motor and brake), followed by conducting simulations to verify whether the formulated hypothesis is correct or not:

1. Hypothesis 1: the behavior of Joint 2 is influenced by the distribution of mass of all components located downstream of it. Assuming all components downstream of Joint 2 are ideally modeled as a single rigid body, it is hypothesized that the variation in experimentally measured torque could be caused by the position of *the Center of Mass* of this rigid body over time.

2. Hypothesis 2: the behavior of Joint 2 is affected by the inclination relative to the vertical of adjacent joints, particularly Joints 3 and 4. In other words, it is hypothesized that the variation in experimentally measured torque could be influenced by the angular displacement of Joints 3 and 4 during the simulation.

8.2.1 Analysis of Joint 2 behavior in the Doosan H2515 collaborative robotic arm: first hypothesis

Hypothesis 1: the behavior of Joint 2 is influenced by the distribution of mass of all components located downstream of it.

Therefore, it is necessary to first model all components downstream of Joint 2 (including Part 2) as a single rigid body. In other words, calculate the *Center of Mass* of the rigid body formed by: Part 2, Part 3, Part 4, Part 5, and Part 6 (Figure 7). Subsequently, the trend of the torque measured at Joint 2 as a function of the calculated *Center of Mass* will be studied:

$$COM_{tot} = \frac{A*m_2 + B*m_3 + C*m_4 + D*m_5 + E*m_6}{m_2 + m_3 + m_4 + m_5 + m_6} \qquad \text{(Equation 8.1)}$$

Where:

- m_i represents the masses of the cobot components;
- A, B, C, D, E denote the distances of Parts 2-3-4-5-6's *Center of Mass* from the vertical axis with respect to Joint 2 (Figure 39).

  These were determined using the same method described in paragraph 3.2 for calculating the force arm.
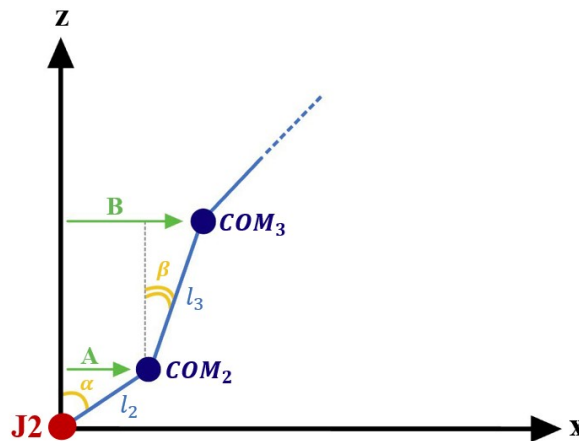

Figure 39 Graphical references for calculating the distances of the centers of mass from the vertical axis

As illustrated in the Equation 8.1, the lever arm is determined as the mass-weighted average of the *Center of Mass* components of each part involved in the calculation.

Afterward, simulations are conducted to assess the torque variation on the joint in relation to the calculated force arm during specific movements. Consequently, two experimental movements are executed:

- Movement of Joint 3 from -120° to 120°, while Joint 2 remains at 0°;
- Movement of Joint 3 from -120° to 120°, with Joint 2 inclined at 20°.

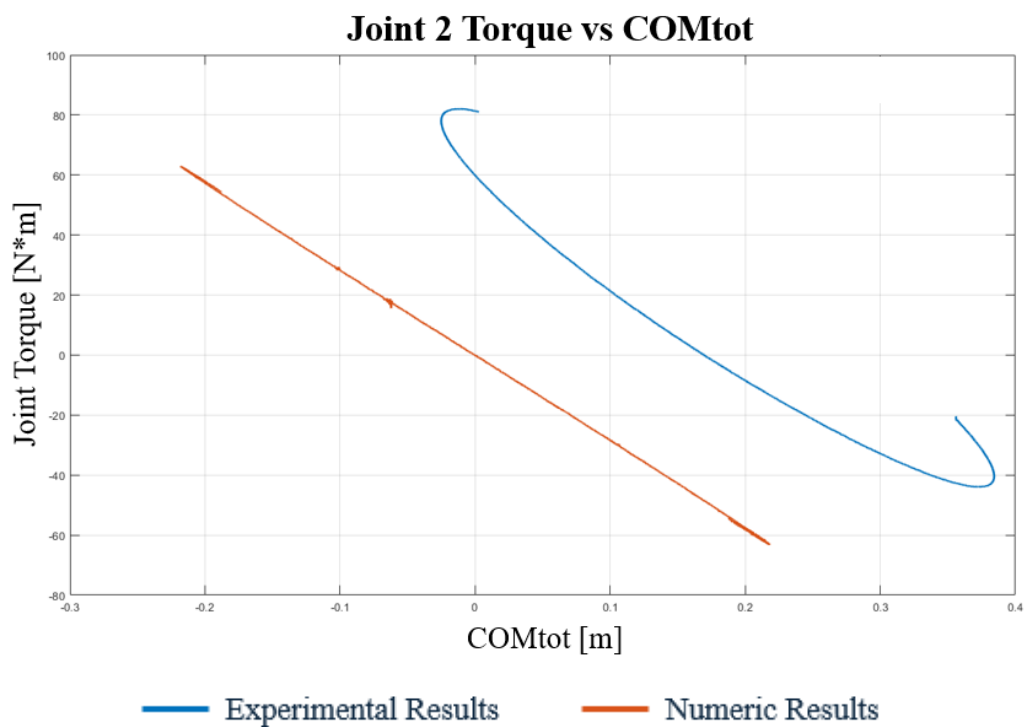The conducted simulations allow for the extraction of the results described in Figure 40:

Figure 40 Joint 2 Torque vs CM_tot

Upon analyzing the torque trend measured at Joint 2 in relation to the *Center of Mass* of the ideal component, it is observed that there is no visible relationship between the examined parameters.

8.2.2 Analysis of Joint 2 behavior in the Doosan H2515 collaborative robotic arm: second hypothesis

Hypothesis 2: the behavior of Joint 2 is affected by the inclination relative to the vertical of the adjacent joints, particularly Joints 3 and 4. As a result, the objective is to assess any potential correlation between the assigned angular displacement of Joint 3 and 4 and the Joint 2 measured torque during a specific simulation.

Specifically, attention is focused on Joint 3 and Joint 4 due to several factors:

1. Lever Effect: the central components of the arm exert a greater lever effect on the joints near the base compared to those at the end. This is due to the shorter distance from Joint 2;

2. Mass Distribution: the masses of the central components are closer to Joint 2 and therefore exert a greater influence. In other words, when the arm is extended, the overall *Center of Mass* is nearer to the central joints than to the end joints, amplifying the effect of mass on the measured torques;

3. Structural Rigidity: the rigidity of the robotic arm tends to be higher in the central segments than at the ends. The segments closer to the base are engineered to sustain heavier loads, thus significantly impacting the torque at joints near the base, such as Joint 2;

4. Force Distribution: dynamic forces exert a greater impact on the central and base joints. When a robotic arm is in motion, torque measurement is influenced not only by gravity but also by dynamic forces generated by movement, such as the acceleration and deceleration of the arm and the load.
   As the arm and the load move, dynamic forces are transmitted through all the joints, progressively accumulating as they approach the base, thus influencing the torque measurement.

For this reason, repeated simulations of a movement of Joint 2 are conducted: a movement from 0° to 90°, at a speed of 1°/s. The low movement speed was chosen to facilitate quasi-static simulations. The advantage of this choice lies in the ability to assume that the movement speed does not influence the parameters of interest.

The distinguishing factor among the various simulations conducted is the initial displacement conditions assigned to joints 3 and 4: movements were executed by setting all possible combinations of inclinations ranging from 0° to 90°, with increments of 10° for the joints considered.

Table 4 provides a summary of the boundary conditions for the conducted simulations:

Table 4 Boundary conditions of Joint 3 and 4 during the 90° movement of Joint 2

Simulation number	Joint 3 initial condition [°]	Joint 4 initial condition [°]
Simulation 1	0	0
Simulation 2	10	0
Simulation 3	20	0
Simulation 4	30	0
Simulation 5	40	0
Simulation 6	50	0
Simulation 7	60	0
Simulation 8	70	0
Simulation 9	80	0
Simulation 10	90	0
Simulation 11	0	10
Simulation 12	10	10
Simulation 13	20	10
Simulation 14	30	10
Simulation 15	40	10
Simulation 16	50	10
Simulation 17	60	10
Simulation 18	70	10
Simulation 19	80	10
Simulation 20	90	10
Simulation 21	0	20
.	.	.
.	.	.
.	.	.

Simulation number	Joint 3 initial condition [°]	Joint 4 initial condition [°]
.	.	.
.	.	.
.	.	.
Simulation 98	70	90
Simulation 99	80	90
Simulation 100	90	90

For clarity of presentation, examples related to several configurations are presented in Figure 41, Figure 42, Figure 43, Figure 44:

Figure 41 Initial condition of Joint 3 and Joint 4 set to 10°

Figure 42 Initial condition of Joint 3 and Joint 4 set to 40°

Figure 43 Initial condition of Joint 3 and Joint 4 set to 70°

Figure 44 Initial condition of Joint 3 and Joint 4 set to 90°

Based on the simulation listed in Table 4, one can derive the trends of both experimental and numerical torque of Joint 2 as a function of its angle, or directly observe the trend of the measured deviation between the results (also as a function of the same parameter). This deviation is calculated as the difference between the numerical value and the observed experimental value for the torque of interest.

The utilization of the second method for illustrating the results might offer enhanced clarity in elucidating the fluctuations of the observed discrepancy.

Figure 45, Figure 46, Figure 47, Figure 48, Figure 49, Figure 50, Figure 51, Figure 52, Figure 53, Figure 54 show the plotted trend of the torque measured on Joint 2:

—— Experimental Results   —— Numeric Results
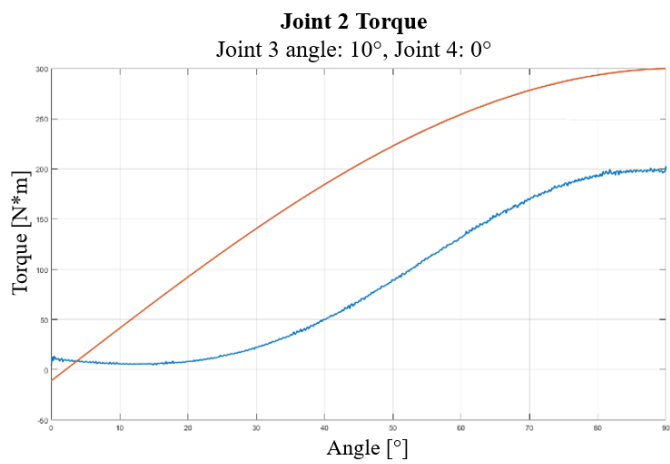
Joint 2 Torque
Joint 3 angle: 0°, Joint 4: 0°
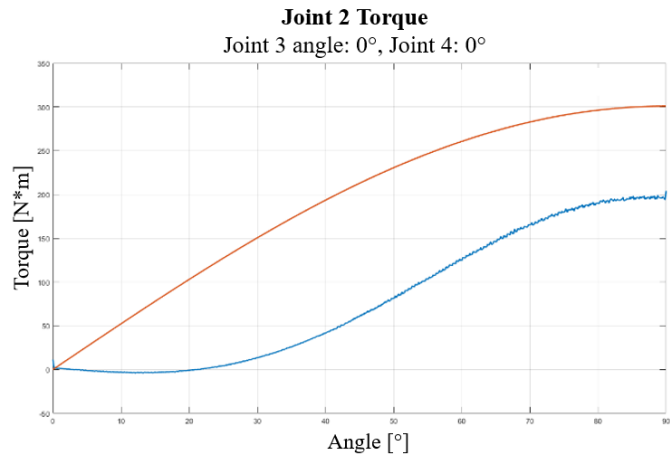
Figure 45 Joint 2 Torque with Joint 3 IC= 0° and Joint 4 IC= 0°

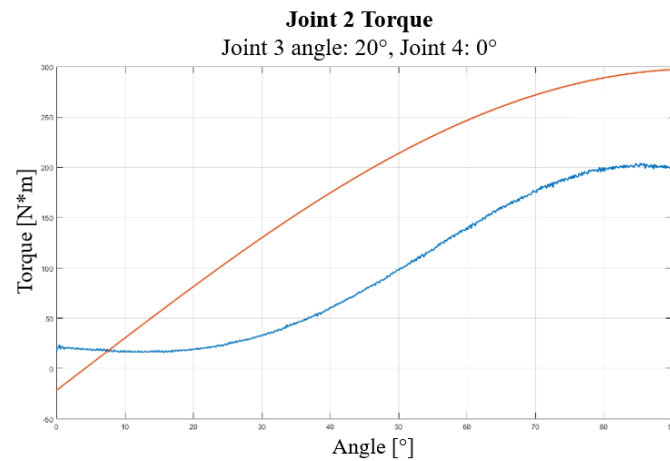**Joint 2 Torque**
Joint 3 angle: 10°, Joint 4: 0°

Figure 46 Joint 2 Torque with Joint 3 IC= 10° and Joint 4 IC= 0°

Joint 2 Torque
Joint 3 angle: 20°, Joint 4: 0°

Figure 47 Joint 2 Torque with Joint 3 IC= 20° and Joint 4 IC= 0°

70

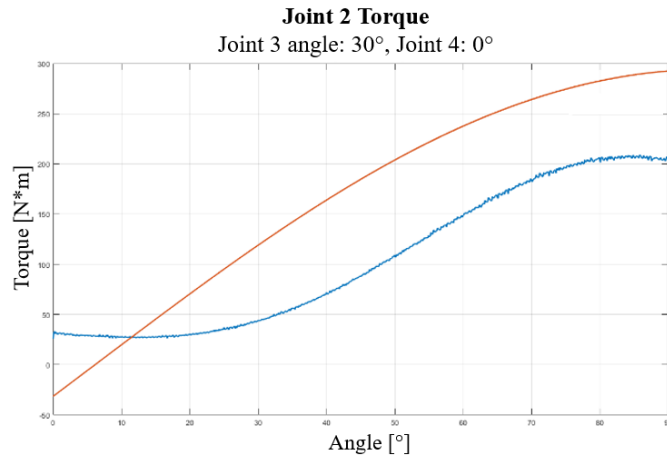**Joint 2 Torque**

Joint 3 angle: 30°, Joint 4: 0°

Figure 48 Joint 2 Torque with Joint 3 IC= 30° and Joint 4 IC= 0°

Joint 2 Torque

Joint 3 angle: 40°, Joint 4: 0°
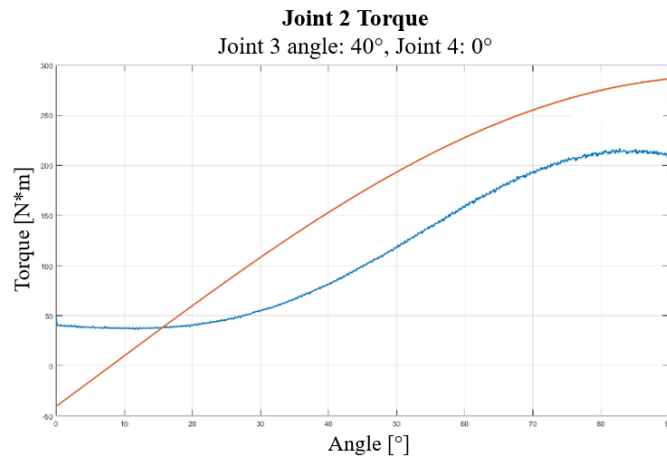
Figure 49 Joint 2 Torque with Joint 3 IC= 40° and Joint 4 IC= 0°

Joint 2 Torque

Joint 3 angle: 50°, Joint 4: 0°
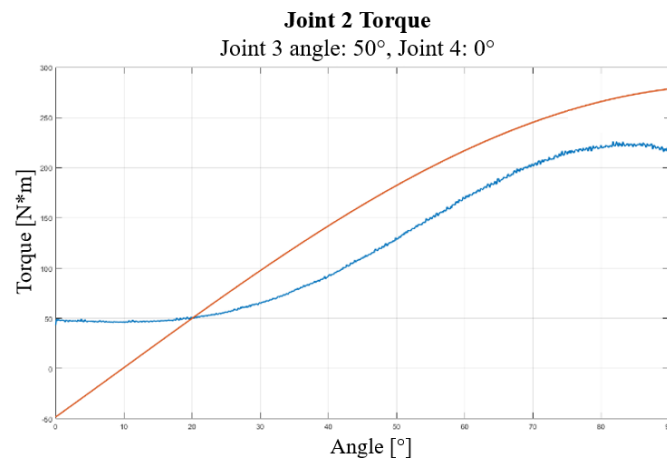
Figure 50 Joint 2 Torque with Joint 3 IC= 50° and Joint 4 IC= 0°

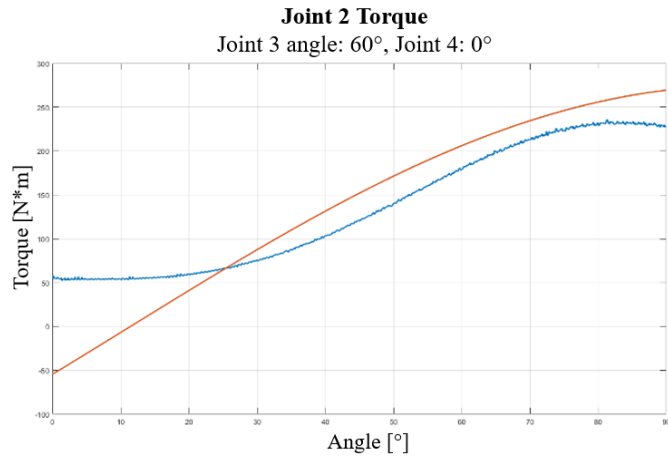**Joint 2 Torque**

Joint 3 angle: 60°, Joint 4: 0°

Figure 51 Joint 2 Torque with Joint 3 IC= 60° and Joint 4 IC= 0°

Joint 2 Torque

Joint 3 angle: 70°, Joint 4: 0°

Figure 52 Joint 2 Torque with Joint 3 IC= 70° and Joint 4 IC= 0°

Joint 2 Torque

Joint 3 angle: 80°, Joint 4: 0°

Figure 53 Joint 2 Torque with Joint 3 IC= 80° and Joint 4 IC= 0°

72

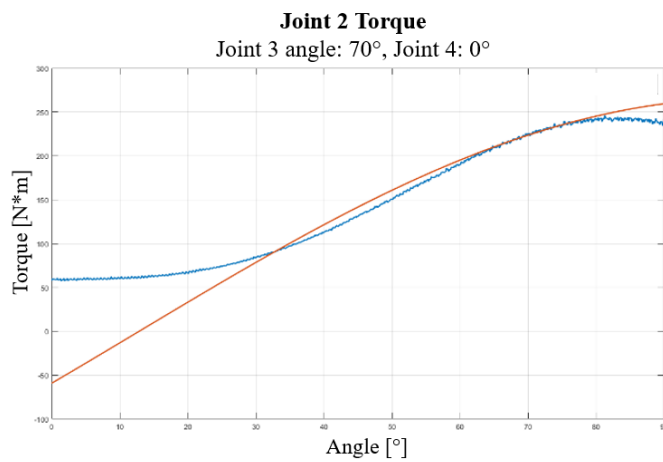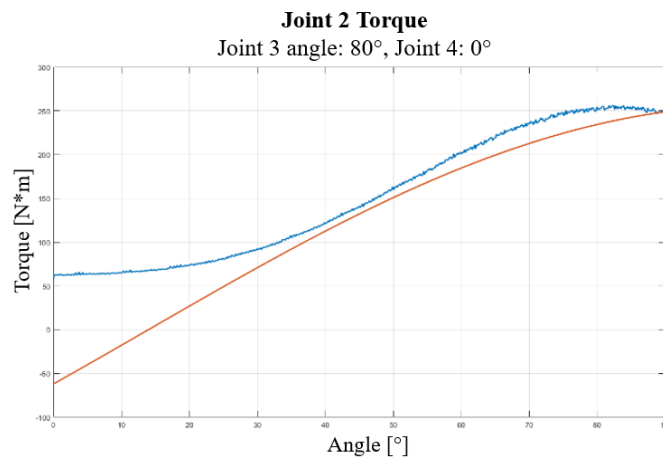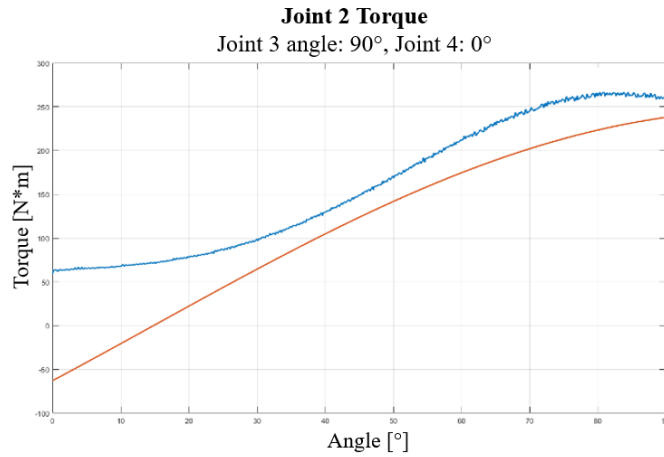*Figure 54 Joint 2 Torque with Joint 3 IC= 90° and Joint 4 IC= 0°*

Figure 55, Figure 56, Figure 57, , Figure 58, Figure 59, Figure 60, Figure 61, Figure 62, Figure 63, Figure 64 directly illustrate the variance between the torque measured on Joint 2 in the numerical and experimental environments, namely the deviation between the obtained results:
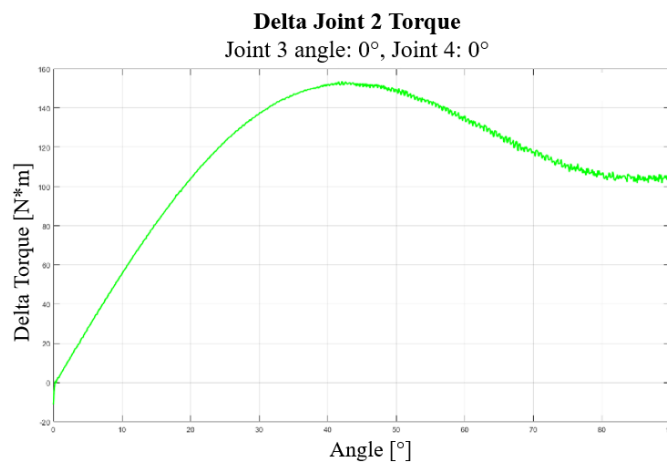

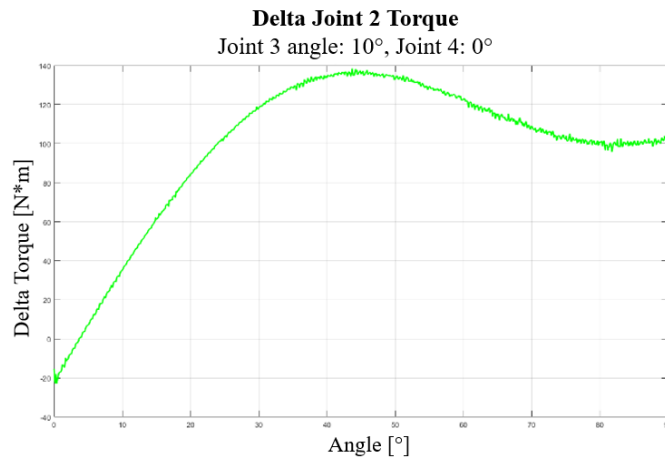*Figure 55 Joint 2 Torques Deviation with Joint 3 IC= 0° and Joint 4 IC= 0°*

Figure 56 Joint 2 Torques Deviation with Joint 3 IC= 10° and Joint 4 IC= 0°
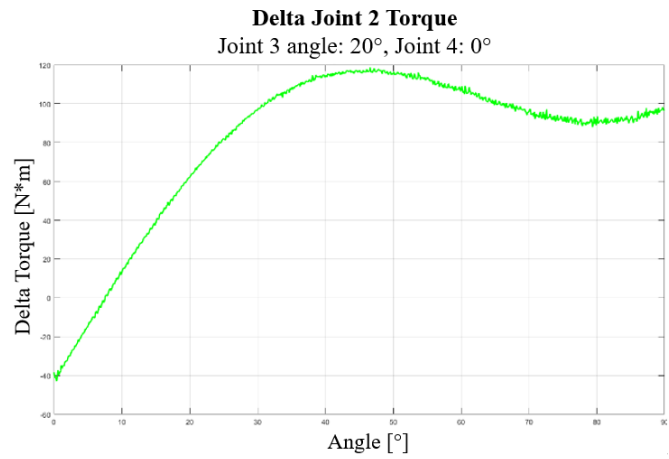
73

Figure 57 Joint 2 Torques Deviation with Joint 3 IC= 20° and Joint 4 IC= 0°

Figure 58 Joint 2 Torques Deviation with Joint 3 IC= 30° and Joint 4 IC= 0°

Figure 59 Joint 2 Torques Deviation with Joint 3 IC= 40° and Joint 4 IC= 0°

Delta Joint 2 Torque

Joint 3 angle: 50°, Joint 4: 0°

Figure 60 Joint 2 Torques Deviation with Joint 3 IC=50° and Joint 4 IC= 0°

Delta Joint 2 Torque

Joint 3 angle: 60°, Joint 4: 0°

Figure 61 Joint 2 Torques Deviation with Joint 3 IC= 60° and Joint 4 IC= 0°

Delta Joint 2 Torque

Joint 3 angle: 70°, Joint 4: 0°

Figure 62 Joint 2 Torques Deviation with Joint 3 IC= 70° and Joint 4 IC= 0°

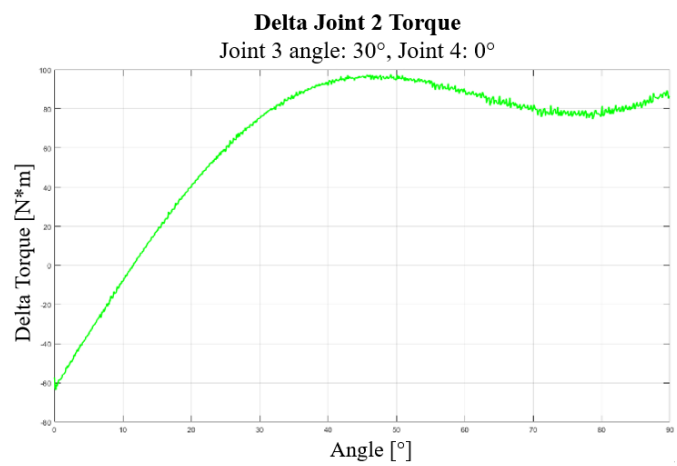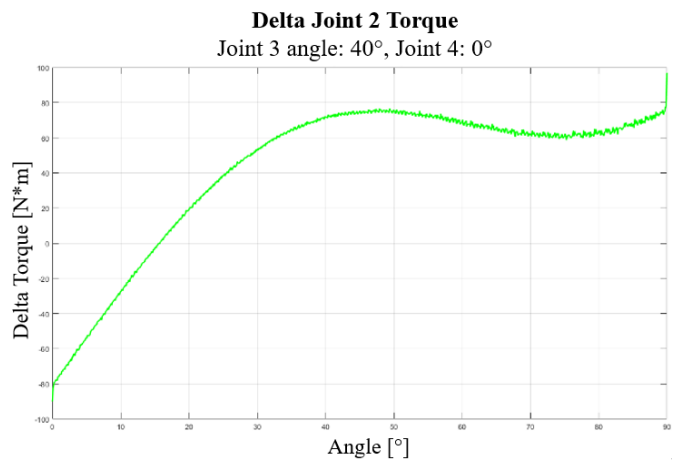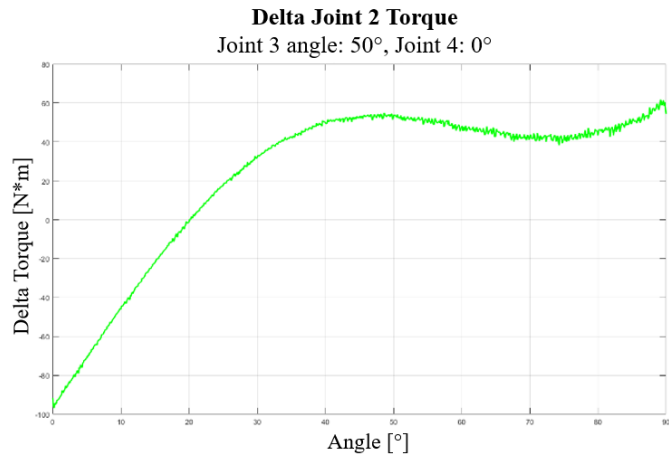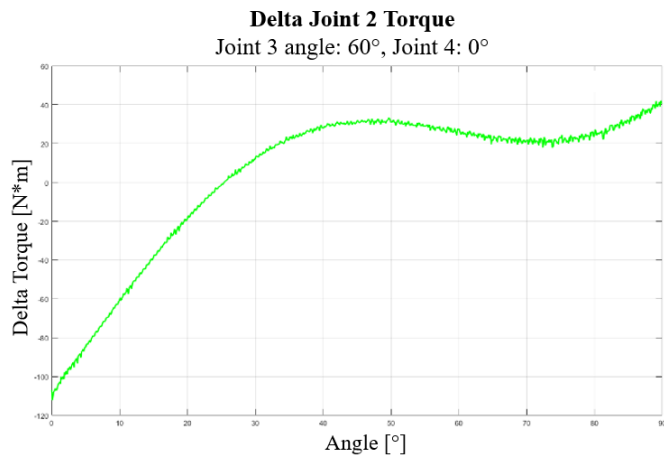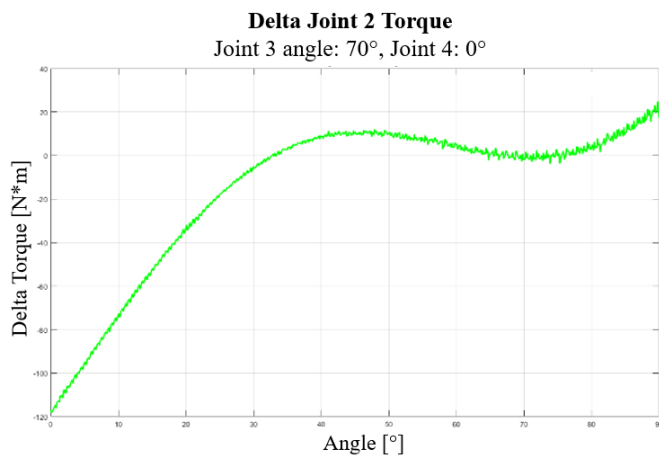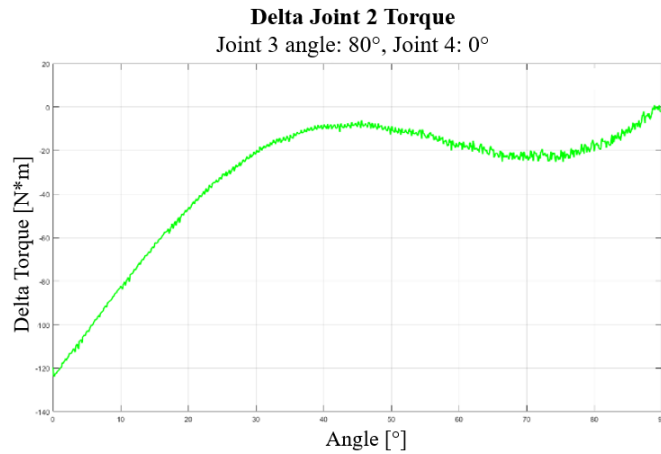*Figure 63 Joint 2 Torques Deviation with Joint 3 IC= 80° and Joint 4 IC= 0°*
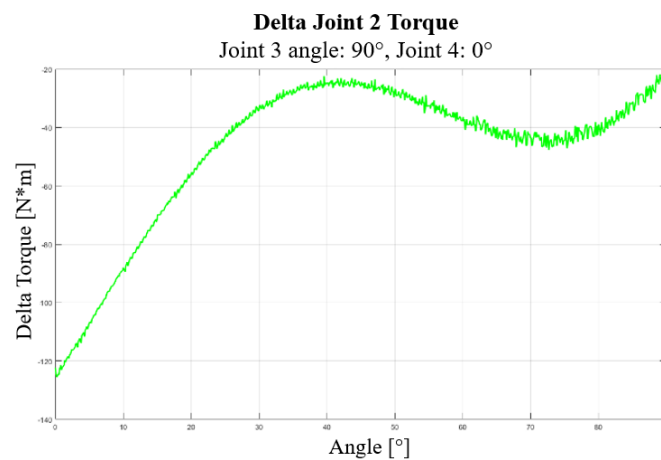

Figure 64 Joint 2 Torques Deviation with Joint 3 IC= 90° and Joint 4 IC= 0°

Figure 55, Figure 56, Figure 57, Figure 58, Figure 59, Figure 60, Figure 61, Figure 62, Figure 63, Figure 64 are referred to simulations 1 – 10 (with reference to Table 4). As the curves representing the relevant quantities for all other simulations display similar behavior, their representation is omitted.

Regarding the results obtained while attempting to verify Hypothesis 2, it is evident that both the torque and the deviation torque relative to Joint 2, as a function of its angle, repeat periodically with varying initial angular displacement conditions assigned to Joints 3 and 4.

In the initial phase of the movement, the deviation increases because, given an initial condition assigned to the joints downstream of Joint 2, its motor must not only rotate the joint but also maintain the assigned condition during the movement. Consequently, it must exert additional effort, leading to the observed increase in deviation.

76

In the final phase of the movement, however, a decrease in the deviation is observed. This occurs because, to initiate the movement, the motor must perform several tasks: alter the system's state of rest by exerting a force sufficient to overcome its inertia, bring Joints 3 and 4 into a different condition from rest by applying an appropriate force, and move Joint 2. However, once the movement has commenced, the motor can focus primarily on rotating Joint 2 while still maintaining the initial conditions assigned to the downstream joints. Furthermore, it is observed that as the initial inclination of Joint 3 increases, the initial deviation grows in the negative direction. In this case as well, the negative sign depends on the formula used to calculate this quantity. Conversely, the final deviation tends to decrease; both phenomena are explained by the same factors mentioned above.

Another noteworthy observation from the analysis of these simulations is a shift in the sign of the experimentally measured torque on Joint 2.

Interestingly, this change in sign does not occur solely at the 0° inclination of the joint; rather, a sign alteration is also evident when the joint angle is approximately plus or minus 20° – this vale depends on joints 3 and 4 initial conditions. Repeating the same motion for Joint 2 but with negative angles would further demonstrate a reversal in its torque sign, occurring around an angle of approximately -20°.

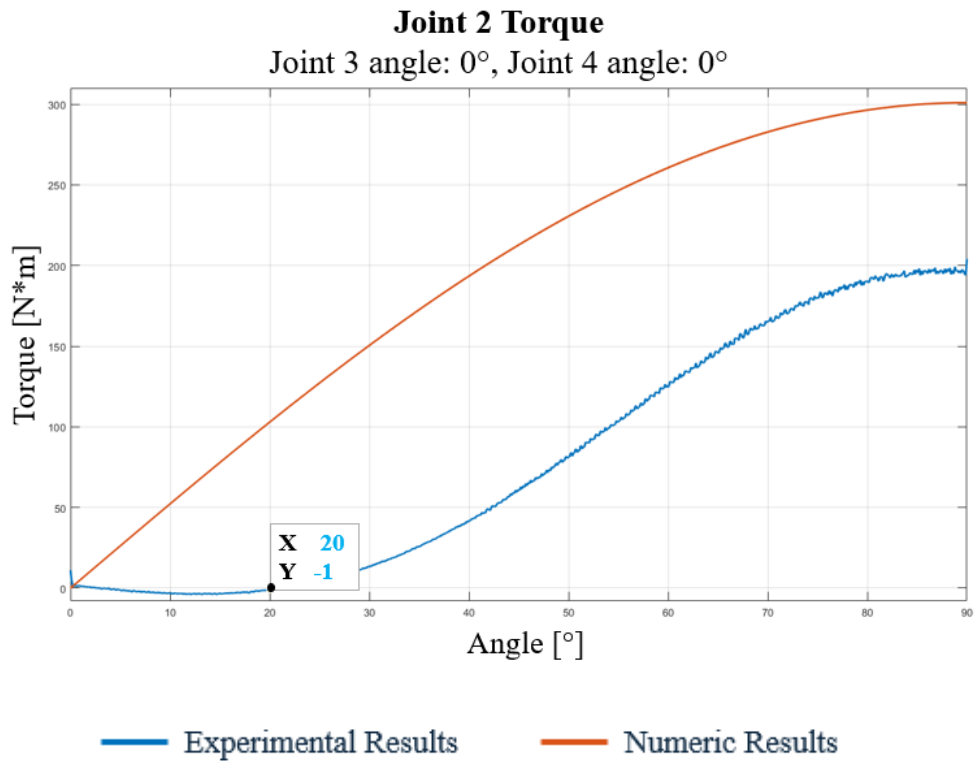Figure 65 depicts this transition occurring at an angle of approximately 20°:
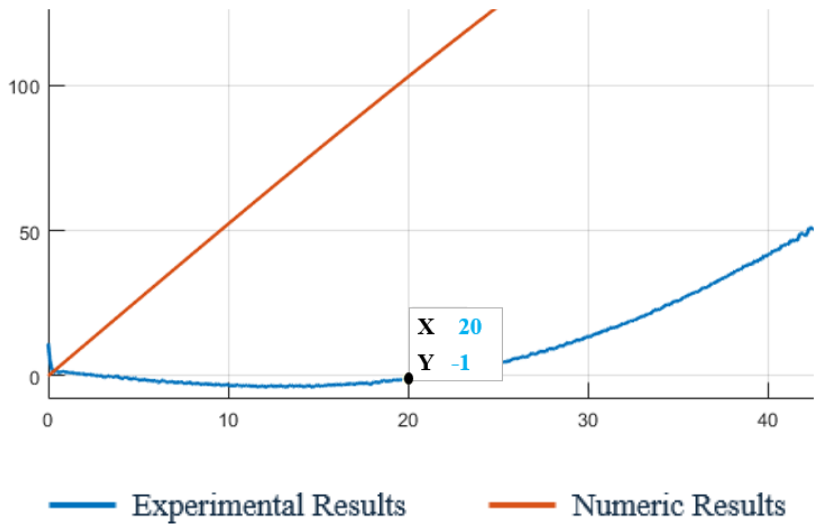
Figure 65 Change in sign of Joint 2 Torque

Figure 66 More detailed view of the change in sign of Joint 2 Torque

78

8.3 Discussion

Analyzing the torque trend measured on Joint 2 in relation to the *Center of Mass* of the ideal component (hypothesis 1), it is observed that there is no evident relationship between the examined parameters. Although not useful in pinpointing the cause of the observed deviation in experimental measurements, this result is valuable for eliminating a factor from the list of potential contributors to the ambiguity in Joint 2's behavior. This allows for a more focused analysis.

Regarding the results obtained in attempting to verify the validity of hypothesis 2, the situation is more complex. It is evident that the torque trend of Joint 2, as a function of its angle, exhibits periodic repetition with various initial angular displacement conditions assigned to Joints 3 and 4. The same pattern is observed when directly comparing the deviation between experimental and numerical torque values as a function of the angle. Consequently, the anticipated result is confirmed: the experimentally measured torque on Joint 2 varies not only with its respective angle but also in relation to the angles of the upstream joints. This fact is further substantiated by the observed change in the sign of Joint 2's torque, occurring not only at 0° but also at different angles, closely tied to the inclinations of the joints proximal to the critical one during motion.

The final step to fully complete the implementation and validation of the digital twin of the collaborative robotic arm Doosan H2515 would be to translate all the theoretical considerations made in this chapter into analytical and quantitative relationships. These relationships will allow for the development of a correction law for experimental data.

Chapter 9

Conclusions and future development

Throughout this experimental research activity, the primary focus was on the implementation and the validation of the digital twin corresponding to the collaborative robotic arm Doosan H2515 produced by Doosan Robotics.

Using the sophisticated *Adams View* software, simulations were created to explore the behavior of the robotic arm in a various range of configurations. These simulated results were then consistently juxtaposed with experimental tests conducted in the laboratory, where the physical cobot operates, using the cutting-edge *DART Studio* platform.

The preliminary phases of the analysis focused mainly on the analysis of the static, kinematic and dynamic movement patterns of the cobot, obtaining overall promising results. These fundamental aspects have been implemented and correctly validated through rigorous experiments and simulations.

However, a notable discrepancy emerged regarding the behavior of Joint 2, particularly evident when the robotic arm assumed unconventional positions or encountered external forces. These inconsistencies between experimental and numerical results have prompted in-depth exploration, with particular attention to unraveling the complexities of the behavior of this fundamental joint.

Different hypotheses were consequently formulated, some of which were then discarded in an attempt to reveal the root causes underlying the ambiguity observed in Joint 2's behavior, ultimately guiding the investigation towards a more refined and focused analysis. However, despite a wide range of simulations aimed at deciphering the factors influencing the experimental torque measured at Joint 2, several limitations have emerged in attempting to derive quantitative relationships. Looking ahead, future research efforts could potentially attempt to translate the qualitative trends of torque measured at Joint 2 into a comprehensive analytical framework, allowing for a deeper understanding of its behavior.

In summary, despite the challenges encountered in fully unraveling the behavioral complexities of the Doosan H2515 collaborative robotic arm, this study represents a noteworthy outlook in the journey towards validation of its digital twin. The insights obtained from the results are very promising for guiding future research efforts aimed at optimizing system performance and formulating more robust control strategies, thus promoting the widespread adoption and safe integration of collaborative robots in modern medical/healthcare contexts.

References

[1] Amarillo, A. Sanchez, E. Caceres, J. *et al.* (2021). 'Collaborative Human–Robot Interaction Interface: Development for a Spinal Surgery Robotic Assistant'. *Int J of Soc Robotics*.

[2] B.J. Grosz, (1996). 'Collaborative Systems', *AI Magazine*, vol.17, no.2.

[3] Bauer, D. Wollherr, M. Buss. (2008). 'Human-Robot Collaboration: A Survey', *International Journal of Humanoid Robotics,* vol. 5, no.1.

[4] Borboni, K. V. V. Reddy, I. Elamvazuthi, M. S. AL-Quraishi, E. Natarajan, S. S. A. Ali. (2023). 'The Expanding Role of Artificial Intelligence in Collaborative Robots', *Machines*, vol. 11, no. 1.

[5] Cesta, A. Orlandini, G. Bernardi, A. Umbrico. (2016). 'Towards a Planning-based Framework for Symbiotic Human-Robot Collaboration', *IEEE 21st International Conference on Emerging Technologies and Factory Automation (ETFA)*.

[6] De Maria, Natale, Pirozzi. (2012). 'Force/Tactile Sensor for Robotc Applications', *Sensors and Actuators A: Physical.*

[7] E. A. Padilla-García, H. Cervantes-Culebro, A. Rodriguez-Angeles, C. Alberto Cruz-Villar. (2023). 'Selection/control concurrent optimization of BLDC motors for industrial robots', *Plos One.*

[8] El Makrini, K. Merckaert, D. Lefeber, B. Vanderborght. (2017). 'Design of a Collaborative Architecture for Human-Robot Assembly Tasks'. *Proceedings IEEE/RSJ International Conference on Intelligent Robots and Systems (IROS).*

[9] F. Vicentini. (2017). *La Robotica Collaborativa: Sicurezza e Flessibilità delle Nuove Forme di Collaborazione Uomo-Robot.*

[10] Isidori. (1986). 'Il Mondo dei Robot: I Protagonisti dell'Automazione Industriale'. Edited by Giunti Barbera.

[11] J.E. Colgate, W. Wannasuphoprasit, M.A. Peshkin. (1996). 'Cobots: Robots for Collaboration with Human Operators', *American Society of Mechanical Engineers, Dynamic Systems and Control Division (Publication).*

[12] Keshvarparast, A., Battini, D., Battaia, O. *et al.* (2023). 'Collaborative robots in manufacturing and assembly systems: literature review and future research agenda', *J Intell Manuf.*

[13] M. Ali. (2012). 'Contribution to Decisional Human-Robot Interaction: Towards Collaborative Robot Companions'. Ph.D. thesis, Institut National de Sciences Appliquées deToulouse, France.

[14] P. Bilancia, J. Schmidt, R. Raffaeli, M. Peruzzini, M. Pellicciari. (2023). 'An Overview of Industrial Robots Control and Programming Approaches', *Applied Sciences,* vol. 13, no. 4.

[15]   S. El Zaatari, M. Marei, W. Li, Z. Usman. (2019). 'Cobot Programming for Collaborative Industrial Tasks: An Overview', *Robotics and Autonomous Systems*.

[16]   S. Patil, V. Vasu, K. V. S. Srinadh. (2023). 'Advances and perspectives in collaborative robotics', *Discov Mechanical Engineering.*

[17]   S. Sakama, Y. Tanaka, A. Kamimura. (2022). 'Characteristics of Hydraulic and Electric Servo Motors', *Actuators*, vol. 11, no. 1.

[18]   S. Thrun. (2004). 'Toward a Framework for Human-Robot Interaction', *Human–Computer Interaction.*

[19]   Steinfeld, T. Fong, D. Kaber, L. Michael, J. Scholtz, A. Schultz, M. Goodrich. (2006). 'Common Metrics for Human-Robot Interaction'. *Proceedings of the 2006 ACM Conference on Human-Robot Interaction.*

[20]   T. Chuan, J. Too, F. Duan, R. Kato, T. Arai. (2010). 'Collaboration Planning by Task Analysis in Human-Robot Collaborative Manufacturing System', *Advances in Robot Manipulators.*

[21]   https://www.universal-robots.com/case-stories/gentofte-hospital/

[22]   https://www.doosanrobotics.com/en/products/series/h2515

[23]   https://hexagon.com/company/divisions/manufacturing-intelligence/msc-software

[24]   https://hexagon.com/products/product-groups/computer-aided-engineering-software/adams

[25]   https://motion-drives.com/blog/2020/10/26/factors-to-consider-when-specifying-brakes-for-robotic-applications/

[26]   https://www.homberger-robotica.com/news/innovazione-e-sviluppo-cobot/

[27]   https://www.universal-robots.com/it/robot-collaborativi-o-cobot-cosa-sono-la-guida-definitiva/